



The LCO Outbursting Objects Key Project: Overview and Year 1 Status

Tim Lister¹, Michael S. P. Kelley², Carrie E. Holt², Henry H. Hsieh^{3,4}, Michele T. Bannister⁵, Aayushi A. Verma⁵,
 Matthew M. Dobson⁶, Matthew M. Knight^{2,7}, Youssef Moulane⁸, Megan E. Schwamb⁶, Dennis Bodewits⁸,
 James Bauer², Joseph Chatelain¹, Estela Fernández-Valenzuela⁹, Daniel Gardener¹⁰, Geza Gyuk¹¹, Mark Hammergren¹²,
 Ky Huynh², Emmanuel Jehin¹³, Rosita Kokotanekova^{14,15}, Eva Lilly³, Man-To Hui^{16,17}, Adam McKay¹⁸,
 Cyrielle Opitom¹⁰, Silvia Protopapa¹⁹, Ryan Ridden-Harper⁵, Charles Schambeau⁹, Colin Snodgrass¹⁰,
 Cai Stoddard-Jones²⁰, Helen Usher²¹, Kacper Wierzbos²², Padma A. Yanamandra-Fisher²³, Quanzhi Ye (叶泉志)²

(The LCO Outbursting Objects Key (LOOK) Project),

Edward Gomez²⁴, and Sarah Greenstreet²⁵

¹ Las Cumbres Observatory, 6740 Cortona Drive, Suite 102, Goleta, CA 93117, USA; tlister@lco.global

² Department of Astronomy, University of Maryland, College Park, MD 20742-0001, USA; mshk@astro.umd.edu

³ Planetary Science Institute, 1700 East Fort Lowell Road, Suite 106, Tucson, AZ 85719, USA

⁴ Institute of Astronomy and Astrophysics, Academia Sinica, P.O. Box 23-141, Taipei 10617, Taiwan

⁵ School of Physical and Chemical Sciences—Te Kura Matu, University of Canterbury, Private Bag 4800, Christchurch 8140, New Zealand

⁶ Astrophysics Research Centre, School of Mathematics and Physics, Queen's University Belfast, Belfast BT7 1NN, UK

⁷ Department of Physics, U.S. Naval Academy, 572C Holloway Road, Annapolis, MD, 21402, USA

⁸ Department of Physics, Auburn University, Auburn, AL 36849, USA

⁹ Florida Space Institute, University of Central Florida, 12354 Research Parkway, Partnership 1 Building, Orlando, FL 32828, USA

¹⁰ Institute for Astronomy, University of Edinburgh, Royal Observatory, Edinburgh, EH9 3HJ, UK

¹¹ Adler Planetarium, 1300 S. DuSable Lake Shore Drive, Chicago, IL 60605, USA

¹² Farther Horizons LLC, USA

¹³ Space sciences, Technologies & Astrophysics Research (STAR) Institute, University of Liège, Liège, Belgium

¹⁴ European Southern Observatory (ESO), Karl-Schwarzschild Str. 2, D-85748, Garching bei München, Germany

¹⁵ Institute of Astronomy and National Astronomical Observatory, Bulgarian Academy of Sciences, 72 Tzarigradsko Shose Blvd., Sofia 1784, Bulgaria

¹⁶ Institute for Astronomy, University of Hawaii, 2680 Woodlawn Drive, Honolulu, HI 96822, USA

¹⁷ Macau University of Science and Technology, Macao

¹⁸ American University/NASA Goddard Space Flight Center, Greenbelt, MD 20771, USA

¹⁹ Southwest Research Institute, 1050 Walnut Street, Suite 300, Boulder, CO 80302, USA

²⁰ School of Physics and Astronomy, Cardiff University, Queens Buildings, The Parade, Cardiff CF24 3AA, UK

²¹ The Open University, Walton Hall, Milton Keynes, MK7 6AA, UK

²² Catalina Sky Survey, Lunar and Planetary Laboratory, University of Arizona, 1629 E University Boulevard, Tucson, AZ 85721-0092, USA

²³ Space Science Institute, 4765 Walnut Street, Suite B, Boulder, CO 80301, USA

²⁴ Las Cumbres Observatory, School of Physics and Astronomy, Cardiff University, Queens Buildings, The Parade, Cardiff CF24 3AA, UK

²⁵ Department of Astronomy and the DIRAC Institute, University of Washington, 3910 15th Avenue NE, Seattle, WA 98195, USA

Received 2022 February 28; revised 2022 June 13; accepted 2022 June 16; published 2022 July 26

Abstract

The LCO Outbursting Objects Key (LOOK) Project uses the telescopes of the Las Cumbres Observatory (LCO) Network to (1) systematically monitor a sample of previously discovered over the whole sky, to assess the evolutionary state of these distant remnants from the early solar system, and (2) use alerts from existing sky surveys to rapidly respond to and characterize detected outburst activity in all small bodies. The data gathered on outbursts helps to characterize each outburst's evolution with time, helps to assess the frequency and magnitude distribution of outbursts in general, and contributes to the understanding of outburst processes and volatile distribution in the solar system. The LOOK Project exploits the synergy between current and future wide-field surveys such as ZTF, Pan-STARRS, and LSST, as well as rapid-response telescope networks such as LCO, and serves as an excellent test bed for what will be needed for the much larger number of objects coming from Rubin Observatory. We will describe the LOOK Project goals, the planning and target selection (including the use of NEOexchange as a Target and Observation Manager or “TOM”), and results from the first phase of observations, including the detection of activity and outbursts on the giant comet C/2014 UN₂₇₁ (Bernardinelli–Bernstein) and the discovery and follow-up of 28 outbursts on 14 comets. Within these outburst discoveries, we present a high-cadence light curve of 7P/Pons–Winnecke with 10 outbursts observed over 90 days, a large outburst on 57P/duToit–Neujmin–Delporte, and evidence that comet P/2020 X1 (ATLAS) was in outburst when discovered.

Unified Astronomy Thesaurus concepts: Comets (280); Long period comets (933); Comet volatiles (2162); Asteroids (72); Centaur group (215); Broad band photometry (184); Narrow band photometry (1088); Optical observation (1169); Short period comets (1452); Oort cloud objects (1158); Automated telescopes (121)

1. Introduction

The Las Cumbres Observatory (LCO) supports several large, coherent, multiyear observing programs called Key Projects²⁶

designed to maximize the science outcomes from its global network of telescopes and their unique capabilities. The LCO Outbursting Objects Key (LOOK) Project²⁷ is a 3 yr Key Project using the many robotic telescopes of the LCO network to study the behavior of active small bodies across the solar system. Specifically, the LOOK Project has two main objectives:

1. Use the telescopes of the LCO Network to systematically image and monitor a sample of dynamically new comets (DNCs) that have been previously discovered over the whole sky. These comets are statistically likely to be entering the planetary region from the Oort Cloud for the first time. By studying this population's brightness and morphology changes as they pass through the inner solar system, we can assess their evolutionary state (primitive versus processed), identify targets for immediate or future follow-up (e.g., outburst versus ambient coma composition), and, ultimately, better understand the behavior of these distant members as remnants of the early formation of the solar system. These results will also help optimize the science return of the ESA Comet Interceptor mission (Snodgrass & Jones 2019) by providing a better picture of the evolving activity and behavior of an Oort Cloud comet, the intended target for Comet Interceptor and other future missions, as well as improve our understanding of the interstellar objects that are just beginning to be discovered.
2. Use alerts and other data from the existing sky surveys such as ZTF (Zwicky Transient Facility; Bellm et al. 2019), PS1 and 2 (Pan-STARRS; Chambers et al. 2016), CSS (Catalina Sky Survey), and ATLAS (Asteroid Terrestrial-impact Last Alert System; Tonry et al. 2018b) to search for outburst activity in small bodies (comets, asteroids, centaurs) and rapidly respond to these outbursts with the telescopes of the LCO Network (Brown et al. 2013). These data will characterize each outburst's evolution with time, help assess the frequency and magnitude distribution of outbursts in general, and contribute to our understanding of outburst processes. This will allow us to gain a better understanding of these outbursts on small bodies and the distribution of volatiles across the solar system.

The LOOK Project's observing program began on 2020 July 1 and will run through 2023 July 31. It was designed to exploit the synergy between current and future wide-field surveys (such as ZTF, Pan-STARRS, ATLAS, and LSST Legacy Survey of Space and Time; Ivezić et al. 2019) and rapid-response telescope networks such as LCO. The techniques, data reduction, and analysis software developed during the LOOK Project and demonstrated using the ZTF survey (the main source of transient events) act as an excellent "scale model" and test bed for what will be needed for the much larger number of objects coming from LSST. Here we describe the LOOK Project goals, the planning and target selection (including the use of NEOexchange as a Target and Observation Manager or "TOM"), and the results from the first year of observations.

2. Scientific Goals

Asteroids and comets are small bodies left over from the formation of the solar system. Their preserved interiors and exteriors hold key information on the conditions and processes extant at that early epoch and the processes that have shaped the solar system since then. Understanding the properties of small bodies in our solar system is key to understanding our own origins, as well as giving context to our searches for volatiles and the precursors to life in the large number of exoplanetary systems now being discovered.

Although comets have spent billions of years in the cold stability of the outer solar system, comets do evolve. Their original primitive nature is altered by irradiation by both solar UV photons and galactic cosmic rays (Stern 2003). Once in the inner solar system, heating by the Sun will preferentially cause the loss of the most volatile components (e.g., Prialnik & Rosenberg 2009), while activity itself also drives both physical changes (Jewitt 2004; Veverka et al. 2013; Vincent et al. 2017) and chemical changes (e.g., Huebner et al. 2006; Feaga et al. 2007; A'Hearn et al. 2011; Le Roy et al. 2015) in cometary nuclei. Understanding this evolution is crucial to connecting observed cometary properties back to conditions in the early solar system, which can then be used to constrain elements of solar system dynamical evolution models like the streaming instability-based successors (see e.g., Morbidelli & Nesvorný 2020 for a recent review) to the Nice and Grand-Tack models (Levison et al. 2009; Walsh et al. 2011). Studies of DNCs and cometary outbursts can help greatly in working toward that understanding.

Additionally, there is a growing understanding that some asteroids in the inner solar system are active, evolving objects. The relatively recent discovery of active asteroids, including main-belt comets and disrupted asteroids (e.g., the activity of (6478) Gault detected by ATLAS and ZTF; Ye et al. 2019), has brought greater interest to this area, and studies of these objects can bring additional insights into the evolution of the different subpopulations of small bodies in the solar system (Jewitt et al. 2015). Active asteroids appear to be a diverse population driven by a variety of potential mechanisms, including volatile sublimation (Hsieh et al. 2004, 2011), direct impacts (e.g., Bodewits et al. 2011; Jewitt et al. 2011), and rotation-driven mass shedding (Ye et al. 2019). These mechanisms are central to our understanding of the processes shaping the evolution of asteroids as a whole. Characterizing active asteroids is thus a direct probe of a crucial part of solar system history.

2.1. Dynamically New Comets

The Oort Clouds are one of the main reservoirs of cometary objects in our solar system. Oort Cloud comets with orbital periods >200 yr are termed long-period comets (LPCs); those of this population with nearly parabolic orbits, which suggest that they are entering the inner solar system for the first time, are referred to as DNCs. This classification can be deduced by examining the original semimajor axis, a_0 , i.e., the semimajor axis of the comet's orbit before entering the planetary region. Values of the reciprocal original semimajor axis $1/a_0$ smaller than $4 \times 10^{-5} \text{ au}^{-1}$ indicate that the comet has likely not had a previous pass through the inner solar system (Dybczyński & Królikowska 2015) and is thus a DNC. More sophisticated orbital integrations and analysis of the Galactic potential and stellar encounters are needed (e.g., Dybczyński & Breiter 2022)

²⁷ <https://www.astro.umd.edu/~msk/science/comae/look/>

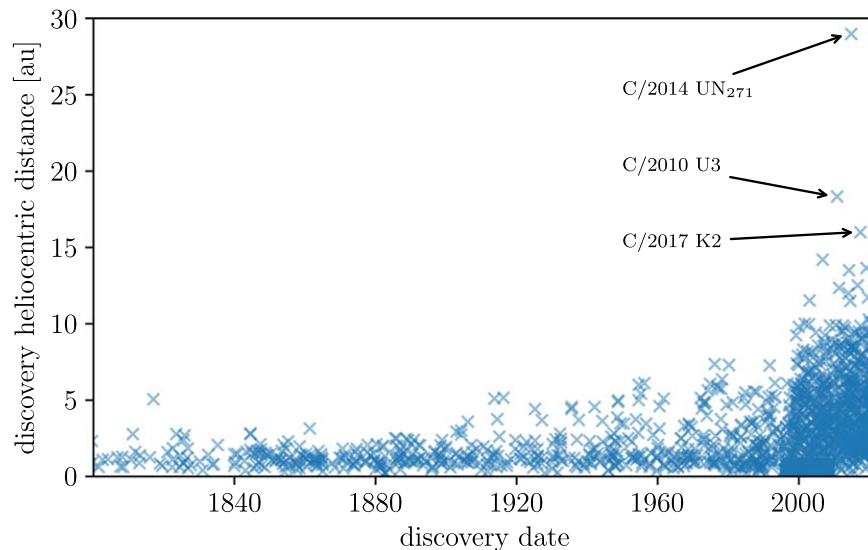


Figure 1. Heliocentric distances at the time of discovery of all the LPCs discovered after 1801 from the MPC database. The density of points increased significantly after 1996, which is when many of the major moving object sky surveys began.

before knowledge of an object’s DNC status can be considered secure, but the use of the $1/a_0 = 4 \times 10^{-5} \text{ au}^{-1}$ value provides an easy-to-implement division for observation planning purposes.

The brightness of a comet is a function of the distances from the Sun and observer but also depends on the amount and type of volatiles and dust in the object. The activity of DNCs at large distances is not well understood. The sublimation of water ice, which typically controls cometary activity closer to the Sun, is inefficient beyond 6 au. Carbon dioxide and carbon monoxide (Yang et al. 2021), more volatile than water and next in order of abundance, are expected to drive activity, including dust emission, at large distances. The small number of comets discovered at ≥ 10 au while inbound, as well as the lack of systematic monitoring, means that the evolution of activity and occurrence of outbursts at greater distances is very uncertain.

Surveys of DNCs have been conducted in the past (e.g., Whipple 1978; Meech et al. 2009), but they have been somewhat limited in either sample size or the range of heliocentric distance that was covered. Current surveys now cover more area to greater depths than ever before, meaning that large numbers of new comets are being discovered and at greater distances from the Sun (Figure 1). This presents us with an opportunity to greatly improve on past work. Coupled with the availability of flexibly scheduled robotic telescopes such as the LCO network, conditions are prime for a systematic study of new comets.

Observations of DNCs will also allow us to better understand the processes that drive cometary activity at distance (e.g., by modeling total dust coma brightness; Meech et al. 2017), allowing better predictions of the behavior of future comets, including mission targets. This is critical for the ESA Comet Interceptor mission (Snodgrass & Jones 2019), which will select its target based on the discovery of a new comet at a large distance but will only meet it years later as it approaches the Sun; success depends on being able to make reliable predictions of how activity evolves in newly identified objects.

2.2. Solar System Object Outbursts

Solar system object outbursts are sudden, short-lived mass-loss events that can span many orders of magnitude in ejection mass and outburst frequency. They vary from small-scale outbursts every few rotation periods (seen by the Deep Impact and Rosetta spacecraft at comets 9P/Tempel 1 and 67P/Churyumov–Gerasimenko; e.g., Farnham et al. 2007; Vincent et al. 2016) to large-scale fragmentation or complete disruption events (e.g., Jewitt et al. 2014; Hughes 1990; Ishiguro et al. 2016). While some outbursts may be caused by sublimation of previously covered pockets of ices with low vaporization temperatures, some have been linked to mass shedding due to rotational instability. Evidence for mass shedding events on asteroids has been provided by the OSIRIS-REx spacecraft, which observed repeated instances of particle ejection (Lauretta et al. 2019). For asteroids with a diameter $\lesssim 1$ km, spin-up via the YORP effect can occur on timescales as little as a million years (e.g., Rossi et al. 2009). As spin rates approach the critical value, sudden structural failure and mass shedding can occur. Even for larger asteroids, small changes in the spin state can rearrange the surface, producing dust events or revealing hidden volatiles (Jacobson et al. 2014).

Distinguishing between types of outbursts and refining physical models requires rapidly detecting outbursts and obtaining time-critical measurements of ejected material within hours or days before it disperses, disintegrates, or sublimates. Characterizing a statistically meaningful sample of the high-amplitude outbursts that can be observed from the ground on large spatial scales will allow connection to the detailed in situ measurements made by spacecraft and the rare super outbursts (e.g., Li et al. 2011 for the super outburst of 17P/Holmes or Ishiguro et al. 2016 for an overview), providing greater understanding of solar system object structure and evolution.

2.3. LOOK Overview

The LOOK Project aims to systematically monitor and characterize a sample of DNCs and obtain rapid-response observations of outbursts, improving our understanding of the

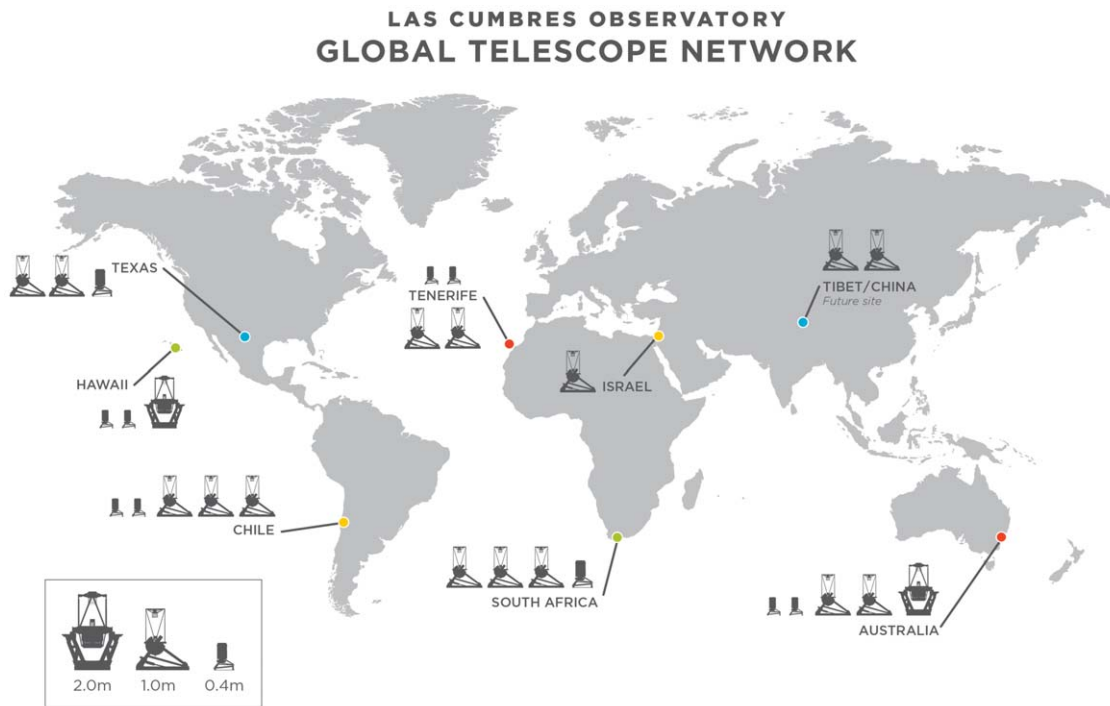


Figure 2. Network map of LCO facilities.

mechanisms responsible for such outbursts. This is achieved by making use of the LCO worldwide network of robotic telescopes which is shown schematically in Figure 2. The main telescopes used by the LOOK Project are the 12 identical LCO designed and built 1 m telescopes at McDonald Observatory (Texas), Tenerife (Canary Islands, Spain), Cerro Tololo (Chile), SAAO (South Africa), and Siding Spring Observatory (Australia). These 1 m telescopes join the two existing 2 m Faulkes Telescopes, Faulkes Telescope North (FTN) in Maui, Hawaii, and Faulkes Telescope South (FTS) in Australia, which LCO has operated since 2005. The whole telescope network has been fully operational since 2014 May, and observations are executed remotely and robotically. Future expansion to a site at Ali Observatory, Tibet, with 1 m class telescopes (which will not be identical to the existing 12 LCO 1 m telescopes) in 2022 is also planned.

The 1 m telescopes have a Sinistro imager consisting of a Fairchild 4096×4096 charge-coupled device (CCD) and Archon controller, giving a $26' \times 26'$ field of view (FOV) with $0''.389$ per pixel and 21 filters. This filter set includes full sets of Bessell (*UBVRI*) and Sloan Digital Sky Survey (SDSS)/Pan-STARRS filters (*ugriz_{sy}*) along with the high throughput Pan-STARRS-*w* (equivalent to $g+r+i$). LOOK Project observations are occasionally supplemented by observations with the 2 m FTN and FTS telescopes through LCO educational partners. The FTN and FTS telescopes originally had identical $10' \times 10'$ FOV CCD imagers with 18 filters, but the imager on the FTN telescope on Maui, Hawaii, was replaced in 2020 November with a copy of the MuSCAT2 (Narita et al. 2019) four-channel instrument called MuSCAT3 (Narita et al. 2020). The MuSCAT3 instrument at FTN makes use of dichroics to provide simultaneous four-color imaging in $g'r'i'z_s$ filters. Each site also has a single high-resolution ($R \sim 53,000$) NRES echelle spectrograph (Eastman et al. 2014; Siverd et al. 2018) with a fiber feed from one or more 1 m telescopes, but these are not used for the LOOK Project. More

details of the telescopes and the network are given in Brown et al. (2013).

To assist in scheduling and tracking the LOOK Project observations, we make use of a target and observation manager system to aggregate observational information on comets and active objects and coordinate follow-up observations. This will be described in more detail in the following sections.

3. Target Selection

The majority of the targets for the DNC monitoring part of the LOOK Project come from new comet discoveries reported from the current wide-field sky surveys (ATLAS, CSS, PS1 and 2, and ZTF). Although these surveys are currently all based in the Northern Hemisphere, they cover down to December $\geq -30^\circ$, providing plenty of coverage for the greater number of LCO 1 m telescopes in the Southern Hemisphere. More discoveries in the Southern Hemisphere will come from the newly commissioned ATLAS 3 and 4 telescopes in Chile and South Africa, respectively.

Targets are automatically ingested by NEOexchange (Lister et al. 2021; see Section 4 for more details) after leaving the Minor Planet Center’s (MPC) NEO or Potential Comet Confirmation pages as confirmed comets. In addition, targets within the NEOexchange database are annotated with a “source subtype” based on their orbit type (Jupiter family, Halley type, parabolic, etc.) during the ingestion process using information from the JPL Small-Body Database or the MPC orbit database. The main discriminator for deciding whether an object is dynamically new is the reciprocal original semimajor axis ($1/a_0$), which is obtained via a query of the Minor Planet Center’s orbital database.²⁸ We use a value of $4 \times 10^{-5} \text{ au}^{-1}$ as the dividing line for considering whether a comet is a DNC. This is used to set a “Dynamically New” source subtype on the

²⁸ https://www.minorplanetcenter.net/db_search/

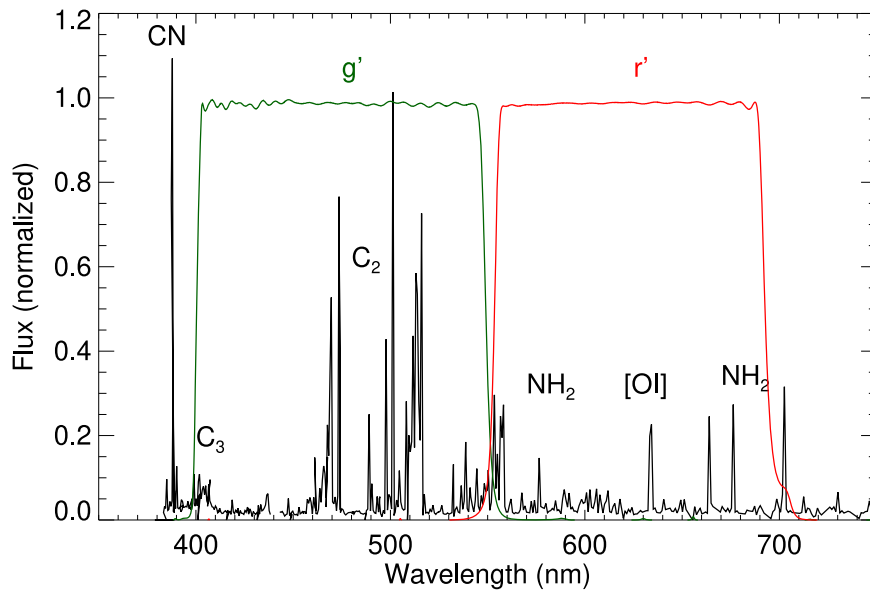


Figure 3. Spectrum of 122P/de Vico (Cochran & Cochran 2002) showing cometary gas emission lines and the overlap with the LCO SDSS/Pan-STARRS g' and r' filters. The continuum was not removed by Cochran & Cochran (2002), as 122P was a very high gas-to-dust ratio comet and the continuum was negligible compared to the emission lines. The r' -filter (red) is free from the strongest cometary gas emission lines, while the g' (green) filter captures many of those. This allows for a good estimate of the different distributions of the gas and dust to be measured separately.

target in the database to aid target selection, but it does not automatically schedule these targets for observations until after manual review. As discussed in Section 2.1, this is somewhat simplistic but allows for easy target selection and an immediate start to observations before a more detailed analysis can become available. Additionally, we consider whether the comet was discovered with a heliocentric distance greater than $r_h \gtrsim 5$ au and will be brighter than $V \sim 20.5$ for long enough to monitor over at least 1 au. Comets that meet the criteria are scheduled for regular monitoring observations (see Section 4). We continue to observe all LOOK Project LPCs, even after a designation of DNC can be confirmed or ruled out. This gives us a longer baseline to compare DNCs with non-DNCs.

Outbursting objects, both comets and asteroids, are by their nature self-selecting targets. Detection of objects in outburst primarily comes from the ZTF survey (see Section 6.3.2) from anomaly detection software (e.g., ZCHECKER; Kelley et al. 2019). This is achieved by looking for deviations from the normal evolution of the magnitude with time or phase and is typically performed automatically by ZCHECKER but can also be performed by manual examination. Other sources of outbursts are always considered, e.g., in the cases of discoveries by amateur astronomers, or other analyses by the team (see 95P/Chiron in Section 6.3.3). In the case of brighter comets, outburst reports often come from the amateur/citizen science community of observers. After assessment of an outburst notification by LOOK Project members, including checking for potential stellar contamination within the photometric aperture, follow-up observations to confirm and study the outburst evolution can be quickly scheduled using the LCO network (see next section) or certain other telescopes (see Section 4.1).

4. Observation Planning and Scheduling

The observing program is controlled through an online portal (NEOexchange; Lister et al. 2021), which is an example of a Target and Observation Manager (TOM). TOM systems handle

the target ingestion and curation, observation scheduling and recording, and serving any resulting data files for a scientifically focused investigation such as LOOK. NEOexchange was developed to handle NEO candidate follow-up and target characterization and had already been operational for several years prior to LOOK, making it the natural place to handle observation scheduling for LOOK. NEOexchange is running in Amazon Web Services (AWS; “The Cloud”), making it available to all the project participants and more reliable (since it is not running on a single server with a single network connection to the outside world).

The photometric monitoring of DNCs takes place every three days using two filters (SDSS/Pan-STARRS g' and r') in order to be sensitive to the gas and dust components of the comet. In Figure 3, we show a spectrum of the extremely gas-rich comet 122P/de Vico at 0.66 au from the Sun (Cochran & Cochran 2002) and spectral throughputs for the g' and r' filters. The r' band is mostly free of gas emission lines and is thus a good proxy for variations in the amount of dust surrounding the nucleus. In contrast, the g' filter covers the strong C_2 and C_3 emission bands. Molecules produced in the coma, including C_2 and C_3 , tend to have spatial profiles shallower than the dust coma (the latter nominally decreases proportional to distance from the nucleus, $\propto \rho^{-1}$). Thus, the $g - r$ color of a comet, as well as its variation with distance to the nucleus ρ , can be used to assess the dust-to-gas ratio of the coma.

NEOexchange has a LOOK-specific summary page that shows newly discovered comets from the sky surveys (as discussed above in Section 3) along with the current monitoring targets. The summary page shows the state of the ongoing monitoring, as well as providing a brief view of the observational circumstances (sky position, magnitude, on-sky motion rate, and heliocentric distance). The LOOK summary page also provides links to visualization plots that allow the evolution of sky position (in equatorial and galactic coordinates), heliocentric and geocentric distance, magnitude, elongation, and Moon separation, along with the visibility

from representative sites in the LCO network in the Northern and Southern Hemispheres.

The LOOK summary page and NEOexchange allow monitoring of outburst targets to be quickly scheduled on the LCO network through a target scheduling form that calculates visibility windows and estimates exposure times based on the brightness and rate of motion, although this is less critical for the slow-moving comets of LOOK than the original NEO targets of NEOexchange. LOOK DNC monitoring observations are scheduled using the cadence features of NEOexchange and the LCO network, which allows a single observing submission to set up the standard month-long observation cadence of 2×180 s exposures in each of Sloan g' and r' every three days.

For outbursting objects, a key component of the LOOK program and a strength of the robotic, rapid-response LCO network is to first validate these outbursts before triggering Target of Opportunity requests on larger, slower facilities (including Hubble Space Telescope) and second characterize the evolution of the post-outburst light curve. Dust moving with radial speeds of $1\text{--}100$ m s⁻¹ will travel $0.''1\text{--}10.''$ day⁻¹ for targets a distance of 1 au from Earth. Thus, the outburst signal within small photometric apertures decays on day to week timescales. Gas timescales are faster, given that it nominally moves near 1 km s⁻¹ (e.g., Tseng et al. 2007; Ishiguro et al. 2016; Opitom et al. 2016). Generally, outbursts are at best discovered within 1–3 days of onset, and therefore the LOOK Project follow-up observations will best characterize the dust. However, if a suitable outburst can be detected in a high-cadence survey (or part of a survey), there is the possibility that gas can be observed and its dynamics characterized with LCO and LOOK. Finally, outbursts may be followed by additional events, or by the appearance of fragments (moving $\lesssim 1''$ day⁻¹), motivating observations beyond the initial light-curve decay.

Follow-up observations of outbursts therefore normally consist of a 10-day-long monitoring with the LCO 1 m telescopes, starting with higher-cadence sampling (every 3 hr) until two days after the outburst discovery, when expected changes are the largest owing to devolatilization and dispersion of the dust and the changing photochemistry of the gas. After this initial intensive monitoring, we switch to a slower cadence of once every 8 hr, which is the approximate spacing between the different nodes in the LCO network (particularly in the Southern Hemisphere). The data from the slower cadence are essential for detecting any disintegration and separation of potential fragments and for characterizing the shape of the light curve, which can be used later to characterize the dynamics and size distribution of the dust ejecta, which leads to an improved estimate of the total mass ejected in the outburst.

Outburst response observations also take place in the SDSS g' and r' filters but with shorter exposure times, typically 60 s, but more exposures in each filter. The exposure times are shorter for the outburst observations to minimize the elongation of the reference stars and less accurate astrometry and photometry caused by the telescope tracking at the object's rate of motion at each visit. This elongation can be more significant for outbursts than for the DNC monitoring. This is because outbursts typically happen in the inner solar system when the object's on-sky motion is higher and therefore exposure times need to be shorter to avoid trailing the reference stars. Observations from LCO Key Projects such as LOOK have a higher priority than the majority of other programs in

Table 1
Targets Observed in MOA-R at Mount John Observatory

Name	$1/a_0^a$ (au ⁻¹)	N^b	r_0^c (au)	q^d (au)	T^e (TDB)
189040	...	1	1.02	0.85	2022-01-21
2009 CD	...	3	1.1	0.66	2020-07-14
2020 UB5	...	4	0.98	0.97	2019-10-12
2021 CA1	...	3	1.02	0.99	2021-03-05
2021 CD1	...	3	1.14	0.58	2020-07-03
2021 CH	...	4	1.08	0.97	2021-03-06
2021 CM	...	5	1.02	1.02	2021-01-29
2021 CP	...	3	0.99	0.99	2017-09-20
2021 CS	...	2	1.03	0.92	2022-01-08
360502	...	1	1.05	0.70	2021-09-10
C/2014 UN271	0.000 141	5	20.74	10.94	2031-01-25
C/2017 W2	0.072 955	2	8.4	3.95	2017-11-01
C/2018 F4	0.001 391	3	10.85	3.44	2019-12-04
C/2019 E3	0.000 030	4	11.66	10.31	2023-11-12
C/2020 R7	0.000 050	3	6.24	2.96	2022-09-16
C/2021 A2	0.004 282	1	1.41	1.41	2021-01-22
C/2021 A6	0.000 022	3	7.95	7.93	2021-05-05
C/2021 A7	0.000 318	6	2.86	1.97	2021-07-15
C/2021 B3	0.030 214	4	2.23	2.16	2021-03-10
C/2021 C5	0.000 037	1	7.23	3.24	2023-02-10
C/2021 G2	0.000 004	1	10.55	4.98	2024-09-10
C/2021 S3	0.001 919	2	10.7	1.32	2024-02-18
C/2022 A2	-0.000061	2	7.79	1.74	2023-02-18
P/2020 V3	...	3	6.23	6.23	2021-02-09
P/2020 V4	...	1	5.14	5.15	2021-07-18

Notes.

^a According to MPC database.

^b Number of visits.

^c Heliocentric distance at the first visit.

^d Perihelion distance.

^e Time of perihelion.

the LCO scheduler, but for responding to outbursts we also have a fraction of allocated time in “Time Critical” mode. This gives a $\sim 33\times$ boost in priority when observation requests are being considered by the LCO scheduler. This is used during outburst follow-up to ensure early-time data for the case of an outburst discovered very soon after onset (as discussed above).

4.1. Follow-up with the Mount John Observatory

The 1.8 m telescope at the University of Canterbury's Mount John Observatory (MJUO) in Takapō, New Zealand (1029 m elevation, MPC code 474), has observed since 2020 December in support of the LOOK program. MJUO adds additional capacity for LOOK follow-up, along with a certain amount of buffer to bad weather at LCO's Australian site, for targets under daily (or more frequent) monitoring. The additional aperture can produce higher signal-to-noise ratio on fainter targets than the LCO 1 m facilities. It also provides a test bed for how classically scheduled and manually operated telescopes can be integrated into the time domain follow-up infrastructure and TOMs. Targets are obtained through the NEOexchange web portal (Lister et al. 2021) and manually scheduled for in-person observation. Observations are made with the 2.2 deg² MOA-cam3 in the MOA-R broadband filter (632–860 nm; Sako et al. 2008). For instance, between 2020 December and 2021 February, 25 targets, comprising 23 comets and 2 active asteroids, were imaged on 10 separate epochs (Table 1). The data for these observations are currently under analysis, with

MOA-R magnitudes converted to r_{P1} magnitudes via color corrections implemented in the `calibrimbore`²⁹ package.

5. Data Processing

Newly acquired images from the LOOK Project from the LCO network are automatically pipeline processed in near real time by the LCO Beautiful Algorithms to Normalize Zillions of Astronomical Images (BANZAI) pipeline (McCully et al. 2018). The BANZAI pipeline performs the standard processing tasks (bias and dark subtraction and flat-fielding correction) to produce a basic calibrated data (BCD) product and additionally performs both an astrometric solution and (since 2021 September) photometric zero-point determination. Processed data products are retrieved from the publicly available LCO Science Archive (which is also located in AWS). These data feed a pipeline at the University of Maryland that performs the domain-specific processing needed for solar system and extended objects.

The comet outburst pipeline periodically queries the archive for new observations and downloads calibrated data as needed. A post-download script processes new images one by one, including background removal, and performs photometric calibration of the frames with the ATLAS-RefCat2 all-sky photometric catalog (Tonry et al. 2018b) using the CALVIACAT software (Kelley & Lister 2021) and background field stars as measured by LCO’s BANZAI pipeline. ATLAS-RefCat2 uses the PS1 photometric system, and the comet outburst pipeline considers a color correction owing to the difference between the PS1 filters and the SDSS/Pan-STARRS filter set used at LCO telescopes (the LCO versions of the SDSS/Pan-STARRS filters have higher and more uniform transmission owing in part to their smaller physical size; compare the filter profiles in Figure 3 with Figure 2 of Tonry et al. 2012). Based on LOOK Project photometry, we derived the following color corrections to convert instrumental g' and r' photometry into g_{P1} and r_{P1} magnitudes:

$$\begin{aligned} g_{P1} - g'_{\text{inst}} &= -0.0863 (g_{P1} - r_{P1}) + ZP, \\ r_{P1} - r'_{\text{inst}} &= +0.0212 (g_{P1} - r_{P1}) + ZP, \end{aligned} \quad (1)$$

where ZP is the best-fit magnitude zero-point for the image. The g_{P1} and r_{P1} color corrections are based on the analysis of 1008 and 1147 images (standard deviation 0.035 and 0.018 mag), respectively. Based on these results, we have proceeded with a fixed color correction for all g' and r' images. The 50th and 90th percentile calibration errors in our initial data set are 0.036 and 0.067 mag for the g band (2175 images) and 0.044 and 0.084 mag for the r band (3228 images), respectively. With the commissioning of additional ATLAS survey facilities in Chile and South Africa, we can hope for a more uniform reference catalog with somewhat greater photometric precision for fainter stars for the southernmost declinations in a later revision of the ATLAS-RefCat without the reprocessing of APASS DR9 survey (Henden et al. 2016) data performed for ATLAS-RefCat2 (Tonry et al. 2018a, their Section 3.3). This potential nonuniformity in the reference catalog zero-points in the far Southern Hemisphere is not a significant source of uncertainty on LOOK comet magnitudes.

Images where the target is missed or the image has other processing issues (missing WCS solution, too few stars for calibration) are automatically saved to a list of files to ignore. Manual inspection is required to identify some other common issues, such as photometric interference from background sources, or scattered lunar light. If the image can be calibrated, then photometry is attempted on the comet centroid or the ephemeris position if centroiding fails. After the target has been measured in the individual frames, data are clustered together by time and telescope (i.e., observing block, median $\Delta t = 870$ s), and the respective photometry and images are averaged together by filter.

6. Results³⁰

6.1. DNCs

The results for the main DNC monitoring part of the LOOK program will be the subject of additional papers (C. Holt et al. 2022, in preparation), but a brief summary of the initial results will be presented here, along with discussion of the special case of the newly discovered “extreme” comet C/2014 UN₂₇₁ (Bernardinelli–Bernstein).

In the first ~ 16 months, LOOK has monitored 15 LPCs with an average data set spanning 265 days (see summary in Table 2). Of the 15 LPCs, 8 currently have $1/a_0 < 4 \times 10^{-5} \text{ au}^{-1}$, suggesting that they are probably dynamically new. These 15 LPCs have been observed at a broad range (2–12) of the possible 1 m telescopes, with a small spike (four LPCs) observed at the eight 1 m telescopes in the Southern Hemisphere and a smaller spike (two LPCs) observed at the same eight telescopes plus the two on Tenerife, Canary Islands. To highlight some early results, beginning in the second half of 2020, we have been monitoring returning comet C/2019 L3 (ATLAS) and the DNC C/2020 R7 (ATLAS) (Figure 4). Using $Af\rho$, an aperture-independent quantity used as a proxy for dust production (A’Hearn et al. 1984), we find that these comets exhibit different brightness behaviors as they approach perihelion. $Af\rho$ is the product of the albedo “A,” the filling factor “ f ” (i.e., how much the total cross section of grains fills the FOV), and the radius of the photometric aperture “ ρ .” C/2019 L3 exhibited a power-law increase in activity with decreasing heliocentric distance, typical of returning comets, while C/2020 R7 first exhibited an activity increase that plateaued as the comet crossed 5 au. DNCs are known to have a much shallower increase in activity (e.g., A’Hearn et al. 1995). However, the details of the brightness behavior, particularly at large heliocentric distances, are not well characterized or understood.

As examples of observations to come, we have recently begun monitoring LPCs C/2021 S3 (PANSTARRS) and C/2021 T4 (Lemmon) starting with heliocentric distances of $r_h \gtrsim 8.5$ au that will eventually reach perihelion below 1.5 au. Currently, C/2021 T4 is designated as dynamically new, while C/2021 S3 is not. With LOOK, we will be able to directly compare the brightness behavior of these objects as they move into the region where water sublimation becomes an efficient driver of activity.

²⁹ <https://github.com/CheerfulUser/calibrimbore>

³⁰ Dates and times of observations in this section are in the UTC time system, except where noted, e.g., for times of perihelion, which are in TDB.

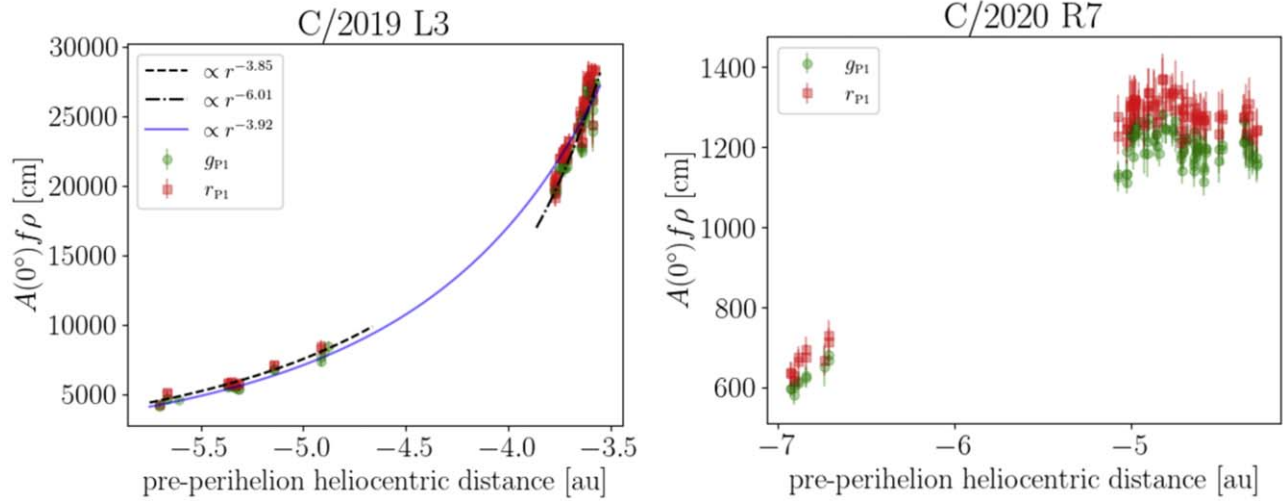


Figure 4. $A(0^\circ)f\rho$ values vs. heliocentric distance (<0 for pre-perihelion observations) for returning comet C/2019 L3 (left) and DNC C/2020 R7 (right), using photometry from LOOK with $5''$ -radius apertures and the g' and r' filters. C/2019 L3 shows a power-law increase in activity (proportional to $r_h^{-3.9}$ overall), whereas C/2020 R7's activity plateaued after an initial increase. Such differences are expected for returning vs. DNCs (e.g., A'Hearn et al. 1995).

Table 2
Monitored LPCs

Name	$1/a_0^a$ (au $^{-1}$)	N^b	r_0^c (au)	q (au)	T^d (TDB)
C/2014 UN ₂₇₁ (Bernardinelli–Bernstein)	0.000050	116	20.16	10.95	2031 Jan 22
C/2019 F1 (ATLAS-Africano)	-0.000066	110	4.55	3.59	2021 Jun 22
C/2019 L3 (ATLAS)	0.000102	57	5.59	3.55	2022 Jan 09
C/2020 O2 (Amaral)	-0.000110	70	5.71	4.86	2021 Aug 28
C/2020 R7 (ATLAS)	0.000028	90	7.03	2.95	2022 Sep 16
C/2020 U4 (PANSTARRS)	0.000021	52	6.57	5.35	2022 Apr 07
C/2021 A1 (Leonard)	0.000375	13	3.55	0.61	2022 Jan 03
C/2021 C5 (PANSTARRS)	0.000037	30	6.78	3.24	2023 Feb 10
C/2021 E3 (ZTF)	0.000033	69	4.82	1.77	2022 Jun 11
C/2021 G2 (ATLAS)	0.000004	50	9.44	4.97	2024 Sep 09
C/2021 O3 (PANSTARRS)	0.000053	50	4.20	0.29	2022 Apr 20
C/2021 P4 (ATLAS)	0.003461	39	4.07	1.08	2022 Jul 31
C/2021 Q4 (Fuls)	0.000147	29	8.46	7.56	2023 Jun 08
C/2021 S3 (PANSTARRS)	0.001919	21	8.60	1.33	2024 Feb 18
C/2021 T4 (Lemmon)	-0.000202	21	8.57	1.48	2023 Jul 31

Notes.

^a According to MPC database.

^b Number of completed visits (through 2022 February 21).

^c Heliocentric distance at the first visit.

^d Time of perihelion.

6.2. C/2014 UN₂₇₁ (Bernardinelli–Bernstein)

One early result from LOOK was the discovery of cometary activity (Kokotanekova et al. 2021; see also Buzzi et al. 2021) around the trans-Neptunian object 2014 UN₂₇₁ at $r_h = 20$ au within 24 hr of the publication of the initial Dark Energy Survey discovery in MPEC 2021-M53 (Bernardinelli & Bernstein 2021) on 2021 June 19. Later analysis of prior TESS data of the now-designated comet C/2014 UN₂₇₁ (Bernardinelli–Bernstein) indicated a large coma in 2018 at 23 au (Farnham 2021) and no detectable rotation period (Ridden-Harper et al. 2021). This comet is unique because of the distance at which it was discovered (as distant as 29 au; Bernardinelli & Bernstein 2021) and its exceptionally large size. Initially estimated to be 75 km in radius (Bernardinelli et al. 2021), Lellouch et al. (2022) recently reported a surface-

equivalent diameter of 137 ± 17 km and a geometric albedo in R band of $p_R = 5.3\% \pm 1.2\%$ using ALMA. This confirms that C/2014 UN₂₇₁ is the largest Oort Cloud origin object ever found by far, being almost twice as large as comet C/1995 O1 Hale-Bopp, and except for the outbursting Centaur 95P/Chiron (Section 6.3.3), the largest known comet in the solar system.

LOOK has been monitoring C/2014 UN₂₇₁ (Bernardinelli–Bernstein) with the LCO network since its announcement, along with Director's Discretionary Time (DDT) imaging and spectroscopic observations using larger telescopes, which will be the subject of later publications (R. Kokotanekova et al. 2022, in preparation). During this time, we have detected an apparent outburst (Kelley et al. 2021c; Table 3) in 2021 September, which will be analyzed in more detail in a forthcoming publication (Kelley et al. 2022).

Table 3
LOOK Project Observed Outbursts

Comet	Discovery Date (UTC)	Δm^a (mag)	ρ^b (arcsec)	Source
Discovery and Follow-up				
7P/Pons–Winnecke	2021 Mar 19.465	-0.23 ± 0.02	5	ZTF; Kelley & Lister (2021)
	2021 Jun 02.06	-1.21 ± 0.06	22	Amateur and ZTF; van Buitenen (2021), Kelley et al. (2021b)
	2021 Jun 05.25	-0.18 ± 0.03	5	LOOK; this work
	2021 Jun 09.60	-0.14 ± 0.03	5	LOOK; this work
	2021 Jun 15.42	-0.34 ± 0.04	5	LOOK; this work
	2021 Jun 22.08	-0.45 ± 0.04	5	LOOK; this work
	2021 Jul 02.61	-0.23 ± 0.07	5	LOOK; this work
	2021 Jul 10.11	-1.10 ± 0.06	5	LOOK; this work
	2021 Jul 18.93	-1.14 ± 0.07	5	LOOK; this work
	2021 Aug 25.64	-0.17 ± 0.09^c	5	LOOK; this work
22P/Kopff	2021 Apr 19.21	-1.12 ± 0.17	5.7	ZTF; Kelley et al. (2021d)
29P/Schwassmann–Wachmann 1	2021 Oct 16.88	-0.21 ± 0.06	5	MISSION 29P; Sharma et al. (2021a)
67P/Churyumov–Gerasimenko	2021 Nov 17.86	-0.64 ± 0.08	5	ZTF; Kelley et al. (2021i)
97P/Metcalf–Brewington	2021 Nov 02.27	-1.5 ± 0.1	15	ZTF; Kelley et al. (2021g)
191P/McNaught	2021 Nov 18.81	-1.64 ± 0.11	5	ZTF; Kelley et al. (2021h)
382P/Larson	2021 Sep 27.23	-0.98 ± 0.09	5	ZTF; Kelley et al. (2021i)
C/2020 R4 (ATLAS)	2021 Apr 24.30	-1.03 ± 0.03	14	ZTF; Kelley et al. (2021e)
	2021 Apr 27.47	-1.14 ± 0.05	14	ZTF; Kelley et al. (2021e)
	2021 May 06.21	-0.60 ± 0.05	14	ZTF; Kelley et al. (2021e)
	2021 Jun 04.22	-1.39 ± 0.07	7	ZTF; Kelley et al. (2021f)
C/2014 UN ₂₇₁ (B-B)	2021 Sep 09.92	-0.65 ± 0.06	4	LOOK; Kelley et al. (2021c)
Follow-up Only				
29P/Schwassmann–Wachmann 1	2020 Sep 25.34	-5.7^d	5.2	MISSION 29P; R.–Miles, report
44P/Reinmuth 2	2021 Jul 13.19	-1.1 ± 0.1	5	ZTF; Kelley et al. (2021k)
57P/duToit–Neujmin–Delporte	2021 Oct 17.74	~ -3	5.8	Amateur; comets-ml msg #30140
	2021 Oct 30	~ -0.9	5	Amateur; comets-ml msg #30180; LOOK ^e
99P/Kowal 1	2021 May 14.18	-0.72 ± 0.06	5	ZTF; Kelley et al. (2021j)
120P/Mueller 1	2021 Aug 08.48	-1.4 ± 0.3	7	ZTF; Kelley (2021)
P/2020 X1 (ATLAS)	2020 Dec 01.46	< -2		LOOK; Fitzsimmons et al. (2020); this work ^f

Notes.

^a Outburst strength measured with respect to the ambient coma. This quantity is aperture dependent.

^b Photometric aperture radius for Δm .

^c The variation in brightness is not statistically significant in this metric, but the outburst is confirmed by inspection of the morphology.

^d Series of outbursts or an extended brightening culminating in the given outburst strength.

^e This was independently announced first as a ~ -0.4 outburst on 2021 November 06.72 in [comets-ml msg #30180](#)

^f Although not identified as an outburst of P/2020 X1 (ATLAS) at the time of discovery by Fitzsimmons et al. (2020), their data suggested an outburst, which is confirmed by our follow-up observations.

6.3. Outbursts across the Solar System

6.3.1. Active Asteroids

Asteroid (248370) 2005 QN₁₇₃, now also designated as comet 433P/(248370) 2005 QN₁₇₃, was discovered to be active on 2021 July 7 by the ATLAS survey (Fitzsimmons et al. 2021). Given subsequently identified archival observations from the Dark Energy Camera on the Blanco Telescope (Chandler et al. 2021) showing that 433P was active during a previous perihelion passage, this object belongs to the subset of active asteroids known as main-belt comets, whose activity is associated with the sublimation of volatile ices (e.g., Snodgrass et al. 2017). The LOOK Project observations using LCO’s network of 1 m telescopes that began on 2021 July 10 form the core of one of the first papers to be published about this object (Hsieh et al. 2021). Here, densely sampled LOOK data (10 visits within the first 38 days after the initial detection of activity) were crucial for tracking the evolution of the comet’s near-nucleus coma, as well as its dust tail. These data

showed that while the coma was fading over the period of observations reported in the paper (2021 July 9 to 2021 August 14 ; perihelion was 2021 May 13), the tail’s surface brightness remained roughly constant, indicating that the tail likely contained larger (and thus longer-lived) particles on average than the coma.

Using additional data obtained by LCO’s Faulkes Telescope North, the Lowell Discovery Telescope, and the Palomar Hale Telescope, Hsieh et al. (2021) also found that the comet’s near-nucleus region and dust tail had similar broadband colors, which implies that no significant gas coma was present. Furthermore, the terminal velocities of ejected dust particles appeared to be extremely low (based on the extremely narrow width of the tail as measured perpendicular to the object’s orbit plane), suggesting that the observed dust emission may be aided by rapid rotation of the object’s nucleus. LOOK observations of this object continued until 2022 January 25 (when the object reached an orbital true anomaly of $\nu \sim 70^\circ$), giving the prospect of potentially being able to place strong

constraints on the turn-off point of the activity, which has not been previously achieved for a main-belt comet.

6.3.2. Comet Outbursts

Within the first ~ 16 months of operation of LOOK we have discovered and/or followed up on 28 outbursts of 14 comets. A summary of all events is given in Table 3. The outburst strengths are expressed as a change in apparent brightness with respect to a previous measurement or the light curve extrapolated to the outburst observation.

Observed outburst strengths range from -0.14 to -5.7 mag. For the smallest events, it is difficult to distinguish between outbursts and normal variability, except that a periodicity would be expected in the latter. Regardless, the LOOK Project data set demonstrates that small transient events may be readily discovered and studied in cometary comae with the LCO network. Analysis of the source of the outburst’s detection in Table 3 shows that the majority (14/28 $\sim 50\%$) have come from the ZTF survey (with LOOK confirmation in the vast majority of cases), with LOOK responsible for 10/28 $\sim 36\%$ and amateur/semiprofessionals contributing the remainder (5/28 $\sim 17\%$). (We consider the 2021 June 02.06 outburst of 7P to have been jointly discovered by both amateurs and ZTF (Kelley et al. 2021b; van Buitenen 2021) and include it in both counts.)

Below we present a high-cadence study of comet 7P/Pons–Winnecke, a follow-up study of a large outburst of comet 57P/duToit–Neujmin–Delporte, and evidence that comet P/2020 X1 (ATLAS) was in outburst at the time of its discovery.

7P/Pons–Winnecke. Comet 7P is a Jupiter-family comet (JFC) in a 6.32 yr orbit with a perihelion distance of 1.23 au. It was discovered on 1819 June 12 and was subsequently lost, rediscovered, and observed numerous times at its close approaches (Kronk 2003). 7P reached its most recent perihelion on 2021 May 27. A small, -0.23 ± 0.02 mag outburst of the comet was observed with ZTF on 2021 March 19.465 and confirmed with prompt LOOK follow-up observations (Kelley & Lister 2021). Following the discovery of a larger, -1.21 ± 0.06 mag event on 2021 June 02.06 (Kelley et al. 2021b; van Buitenen 2021), we initiated our nominal outburst follow-up observation sequence, during which another outburst occurred. With three confirmed outbursts of this comet and the target moving into the southern hemisphere (outside the typical NEO survey regions), we continued with an intensive outburst discovery campaign until 2021 August 31 with a median cadence of 14 hr (full range: 1.3 hr to 4 days). Some additional data on 2021 June 05, 09, and 14 were obtained by Helen Usher and Richard Miles using the LCO 2 m FTN+MuSCAT3 instrument. We also obtained sparse photometry of the comet with the TRAPPIST telescopes (Jehin et al. 2011).

Our assembled post-perihelion light curve based on 5"-radius aperture photometry is presented in Figure 5, including supporting photometry from the TRAPPIST telescopes. More details about TRAPPIST data reduction and image processing are given in Moulane et al. (2018) and references therein. Within our light curve, 10 outbursts have been identified (Table 3; the first 7P outburst was pre-perihelion and therefore does not appear in Figure 5). All events were confirmed based on a visual inspection of the images after subtracting a reference image of the comet either before or after the event. Including an additional -0.29 ± 0.07 mag outburst discovered on 2021 June 7.858 by Sharma et al. (2021b), and not observed

by LOOK, brings the total to 10 outbursts in the 90-day period post-perihelion. Including the pre-perihelion outburst listed in Table 3 and a tentative -0.38 ± 0.12 mag outburst discovered on 2021 February 03.446 by Kelley & Lister (2021), this comet had at least 12 outbursts over a 183-day period.

Aside from the prolific comet 29P/Schwassmann–Wachmann 1 (Trigo-Rodríguez et al. 2008), no other comet has shown evidence for so many outbursts from ground-based data sets. For comet 7P/Pons–Winnecke, the observed outburst frequency is at least partially a consequence of the observational circumstances. Kelley et al. (2021a) proposed an outburst discoverability metric, D , that assesses the difficulty to detect outbursts given a comet’s ambient coma brightness. The motivating argument is that small aperture sizes limit the amount that the ambient coma (an extended source) can dilute the signal from the outburst (which is initially point-source like). Thus, the metric is inversely proportional to mass-loss rate (the higher the mass-loss rate, the more difficult it is to detect an outburst of a given size) and comet–observer distance (the closer the comet, the smaller the aperture projected at the distance of the comet). With the mass-loss rate parameterized by the quantity $Af\rho$, the discoverability metric is

$$D \propto \frac{1}{Af\rho \Delta}. \quad (2)$$

We fit the quiescent $Af\rho$ values for comet 7P with a function proportional to r_h^k and find $A(0^\circ)f\rho = 148r_h^{-0.4}$ cm (plotted in Figure 5). Therefore, the outburst discoverability metric varies from ~ 0.02 to 0.05 cm $^{-1}$ au $^{-1}$ in our data set (median 0.04 cm $^{-1}$ au $^{-1}$). Kelley et al. (2021a) found six outbursts of comet 46P in their light curve of that comet taken during its historic close approach to Earth (perigee = 0.077 au). The D values for 46P ranged from 0.01 to 0.2 cm $^{-1}$ au $^{-1}$ (median 0.08 cm $^{-1}$ au $^{-1}$), and Kelley et al. (2021a) showed that a more typical short-period comet would have values at least 10 times smaller. Comet 46P was already an outlier for the number of outbursts seen at a single comet in telescopic data (see Ishiguro et al. 2016), but given that the outburst discoverability for 46P was more favorable than for 7P, we conclude that the frequency of outbursts at 7P is at least four times larger than observed at 46P (0.066 day $^{-1}$ vs. 0.016 day $^{-1}$).

57P/duToit–Neujmin–Delporte. An apparent outburst of 57P/duToit–Neujmin–Delporte was reported³¹ on the *comets-ml* mailing list by F. Kugel. They reported an apparent brightening of ~ 3 mag based on observations obtained with a 0.4 m telescope on 2021 October 17.74. Investigation of the MPC database constrained the outburst to have occurred between two ATLAS observations on 2021 October 5 and October 14. LOOK follow-up observations started on 2021 October 19.77 show the initial decline from the outburst. LOOK and TRAPPIST-South observations (which began on 2021 November 3; see Figure 6 for the combined light curve) show evidence for an additional outburst around 2021 November 2 (an apparent outburst of ~ 1 mag in the LOOK data on 2021 October 29 is due to stellar contamination with a bright $G = 12.9$ star (Gaia EDR3 4080052973666546176) used here). We searched the Gaia-EDR3 (Gaia Collaboration et al. 2021) catalog for additional contaminating field stars that were

³¹ <https://groups.io/g/comets-ml/message/30140>

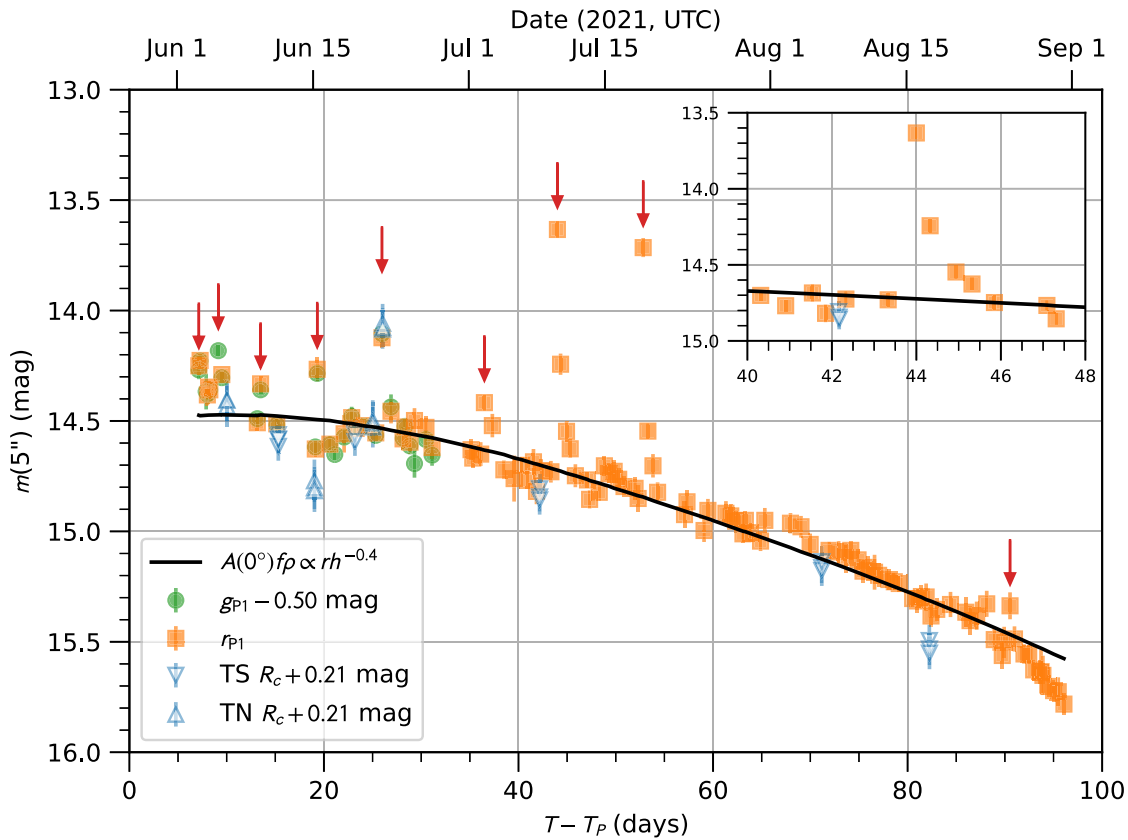


Figure 5. LOOK Project and TRAPPIST light curve of comet 7P/Pons–Winnecke, measured within $5''$ -radius apertures. This plot and the subsequent three show the time on the lower x -axis as a function of time from perihelion. The g_{P1} -band photometry has been offset by the measured color of the inner coma, $g_{P1} - r_{P1} = 0.50 \pm 0.01$ mag, to produce effective r_{P1} -band data. TRAPPIST-South (TS) and TRAPPIST-North (TN) R_c -band photometry has been offset by the color of the Sun: $R_c - r_{P1} = -0.21$ mag (Willmer 2018). An approximate secular trend line is plotted, based on an $Af\rho$ model: $A(0^\circ)f\rho = 148 r_h^{-0.4}$ cm. Arrows mark outbursts of the comet. An inset shows the light curve of the 2021 July 10 outburst in detail.

within a $6''$ radius. The only additional potential contaminants that had $G < 17$ were a $G = 16.6$ star with separation $2''.7\text{--}5''.4$ from the comet on 2021 October 21.38 and a $G = 16.7$ star with separation $5''.3\text{--}5''.6$ from the comet on 2021 October 31.06. We can therefore be reasonably confident that a stellar contaminant is not the cause of any apparent brightening.

The timing of the second outburst is not well constrained. As noted above, our data on 2021 October 29 were contaminated by a bright star and were not usable. We searched the MPC database for additional data around this time but were unable to find any reports of total brightness before 2021 November 5. This lack of data for 2021 October 25 to 2021 November 01, when the first outburst was still declining and the second outburst occurred, makes the amplitude of the second outburst hard to judge. If we assume that the LOOK data from 2021 October 31 at $r_{P1} \sim 13.9$ were during the rise, this puts the outburst onset around 2021 October 30, giving an estimated ~ 0.9 mag increase in brightness from the prior measurement during this time. There was an independent announcement³² on 2021 November 06.72 of what is most likely this outburst by an amateur astronomer as a ~ -0.4 mag outburst measured in a $5''.8$ aperture.

P/2020 X1 (ATLAS). Comet P/2020 X1 is a JFC in a 9.6 yr orbit with a perihelion distance of 2.87 au. It was discovered during the course of the ATLAS sky survey. Fitzsimmons et al. (2020) report discovery, follow-up, and pre-discovery

observations between 2020 December 01 and 08. In the reported photometry, the comet’s apparent magnitude is clearly increasing with time on day-long timescales. LOOK follow-up observations comprise detections on 2020 December 11.035 and 12.081 at $r_{P1} = 19.67 \pm 0.07$ mag and 19.88 ± 0.08 mag, respectively ($5''$ -radius aperture). In Figure 7, we show ATLAS, Pan-STARRS, ZTF, and LOOK project photometry of the comet as absolute magnitude, corrected using the Schleicher–Marcus phase function (Schleicher & Bair 2011). Neglecting bandpass and aperture size differences, the absolute magnitude increases ~ 2 mag over an 11-day period, and more slowly thereafter, suggesting that the comet was discovered during an outburst.

6.3.3. Centaurs

Centaurs are recent escapees from the Kuiper Belt and trans-Neptunian region on giant planet crossing and scattering orbits. They serve as the likely progenitors of the solar system’s JFC population (Duncan & Levison 1997; Di Sisto & Rosignoli 2020). Centaurs have been observed to exhibit comet-like activity, which may be caused by drivers distinct from most short-period comets (e.g., Jewitt 2009; Guilbert-Lepoutre 2012). In 2021 August, the ATLAS survey identified a brightening in 95P/(2060) Chiron’s apparent magnitude that was not consistent with rotational or orbital phase effects. This indicated a possible new cometary outburst or an enhanced phase of cometary activity in Chiron (Dobson et al. 2021a, 2021b). ATLAS observations

³² comets-ml msg #30180

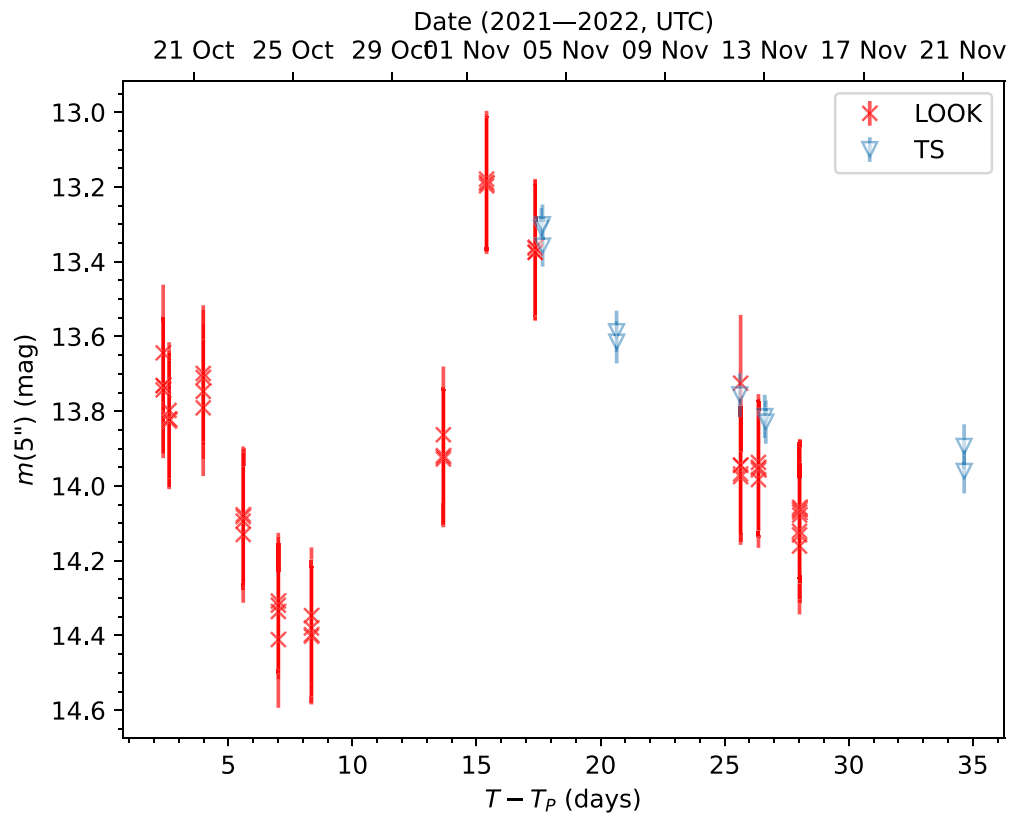


Figure 6. Light curve of comet 57P based on $5''$ -radius r_{p1} -band photometry from the LOOK Project and TRAPPIST-South (TS) R_c -band photometry, which has been offset by the color of the Sun: $R_c - r_{p1} = -0.21$ mag (Willmer 2018). Data from 2021 October 29, which was affected by a bright stellar contaminant, has been removed.

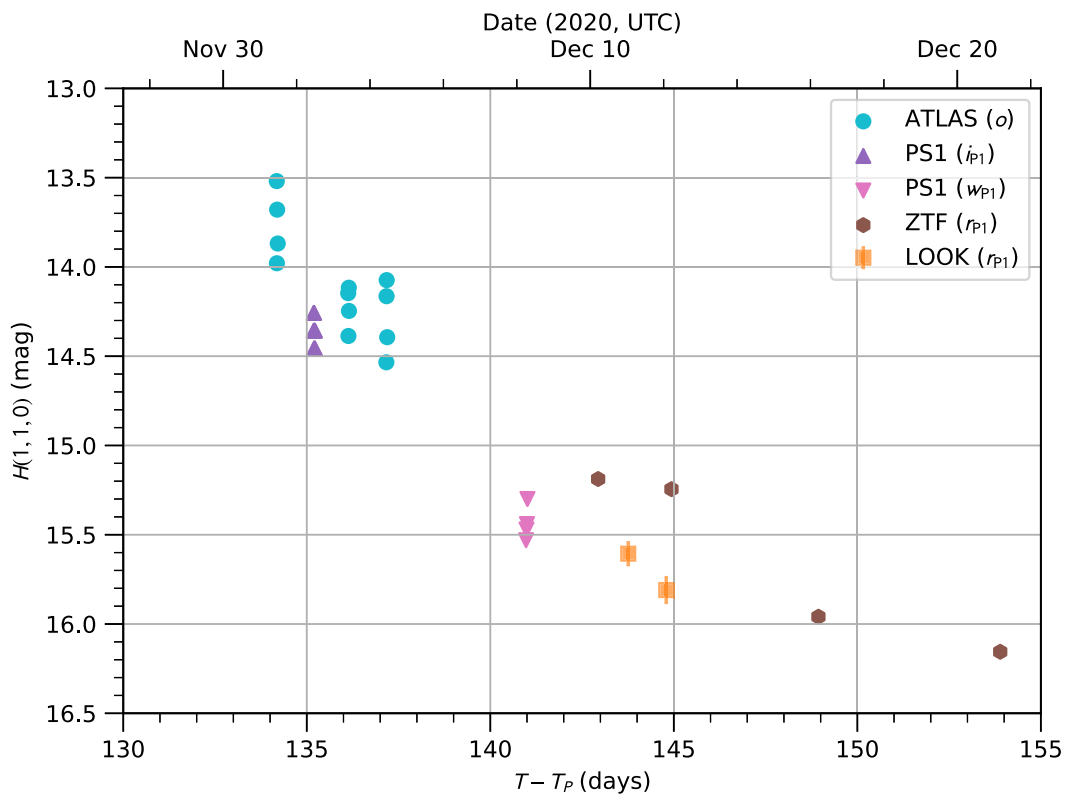


Figure 7. Absolute magnitude of comet P/2020 X1 (ATLAS) based on ATLAS (o band; Tonry et al. 2018b), Pan-STARRS (PS1, i_{p1} and w_{p1} bands; Tonry et al. 2012), and ZTF (r_{p1} band; Bellm et al. 2019) data reported to the Minor Planet Center and $5''$ -radius r_{p1} -band photometry from the LOOK Project. No attempt has been made to correct for different aperture sizes and bandpasses. However, the rapid decline in brightness, suggestive of an outburst, is clear.

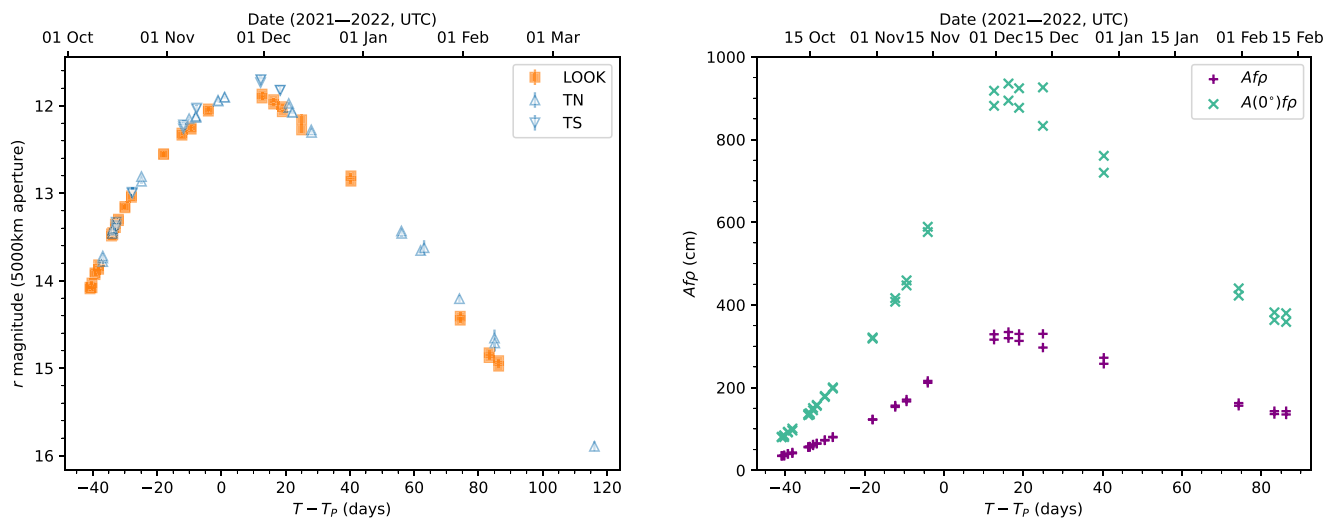


Figure 8. LOOK Project and TRAPPIST light curve (indicated by “TN” for TRAPPIST-North and “TS” for TRAPPIST-South) of comet 156P/Russell-LINEAR, measured within a 5000 km radius aperture at the comet distance. LOOK g_{P1} -band photometry has been offset by the measured color of the inner coma, $g_{P1} - r_{P1} = 0.50 \pm 0.01$ mag, to produce effective r_{P1} -band data. Also plotted (right panel) are the $Af\rho$ and $A(0^\circ)f\rho$ values from LOOK. Both panels show time as a function of time from perihelion ($T_p = 2,455,9171.313576862$ or 2020 November 17 19:31:33 TDB).

found no definitive coma or extended features. As described by Dobson et al. (2021b), four 245 s w -band follow-up exposures were taken on 2021 September 06 using the LCO 1 m telescope at Cerro Tololo Inter-American Observatory (CTIO). The telescope was tracked at Chiron’s on-sky rate of motion, resulting in star trails of $0''.4$ per exposure. The deeper LOOK observations were consistent with the ATLAS data, finding no extended point-spread function (PSF) or visible coma/tail features. It is unclear from the available LOOK data whether this was the start of a brand new outburst or an increase from a baseline activity held constant over the past 6 yr. Deeper exposures and longer-term data will be needed to try to resolve this situation once 95P becomes visible again from 2022 July.

6.4. Other Observations

156P/Russell-LINEAR. 156P is a short-period JFC that had a complicated discovery history (McNaught 2003), having been discovered on four separate occasions with an apparently asteroidal appearance on three of those occasions. The comet has decreased in perihelion distance from $q \sim 1.58$ au in the 2014 perihelion passage to $q \sim 1.33$ au following a close pass (~ 0.36 au) with Jupiter in 2018 March. This has also shortened the orbital period from 6.88 to 6.44 yr. After a report on 2020 October 06 that the comet was found to be brighter than expected³³ and a follow-up note on the perturbation by Jupiter,³⁴ we initiated LOOK follow-up observations. The subsequent data showed that the comet was not in outburst but was undergoing enhanced activity. We continued to observe this comet through 2021 February 12. Photometry of the comet is presented in Figure 8. The LOOK data have been combined with data from the TRAPPIST-North and TRAPPIST-South telescopes (Jehin et al. 2011), which have been transformed from R to r' . The combined light curve, along with $Af\rho$, shows a marked asymmetry in the light curve on either side of perihelion. This behavior could be due to the orientation of the active source regions on the surface of the comet toward Earth

before and after perihelion. The gas activity of the comet shows the same asymmetric shape as the dust activity on both sides of perihelion (Moulane et al., private communication). This kind of asymmetry in the comet’s activity has been seen in many LPCs and JFCs. Narrowband photometry of comet 156P shows clear detection of radicals such OH, CN, C_2 , and C_3 in the optical, indicating that the comet has a typical composition given the ratios of the gas production rates (Jehin et al. 2020).

Figure 9 shows the r' coma evolution with time. The shape of the coma was asymmetric, and it has changed throughout the monitoring window. 156P reached its peak activity on 2020 November 30 (12 days after perihelion), when the coma was the brightest. There are possible hints of substructure in the coma in the 2020 November and December images. Since then, the comet has faded gradually.

We performed a search of the magnitudes reported to the Minor Planet Center and the Comet OBServations (COBS³⁵) database for data from previous perihelion passages. This resulted in 38 observations from 2007 September 11 to 2009 April 19 from the 2007 perihelion and 26 observations from 2013 July 05 to 2015 April 16 from the 2014 perihelion. These are dwarfed in number by the almost 1900 observations (so far) from the 2020 perihelion.

The data from the 2013–2015 apparition, along with the predicted evolution of the total magnitude, are plotted in Figure 10. The JPL Horizons predicted total magnitude uses the IAU model for comet brightness:

$$\text{Total mag.} = M_1 + 5 \log_{10}(\Delta) + k_1 \log_{10}(r),$$

with $M_1 = 12.7$, $k_1 = 8.5$, where Δ and r are the Earth–comet and Sun–comet distances, respectively. An independent fit to all the 1986–2015 data (prior to the current brighter apparition and the encounter with Jupiter) produced a model with $M_1 = 14.3$, $k_1 = 10.0$, which significantly underpredicted the observed brightness during 2013–2015. The data are very sparse and consist mainly of data from the NEO surveys but appear to indicate that the intrinsic brightness of the comet was

³³ <https://groups.io/g/comets-ml/message/29149>

³⁴ <https://groups.io/g/comets-ml/message/29150>

³⁵ <https://www.cobs.si/>

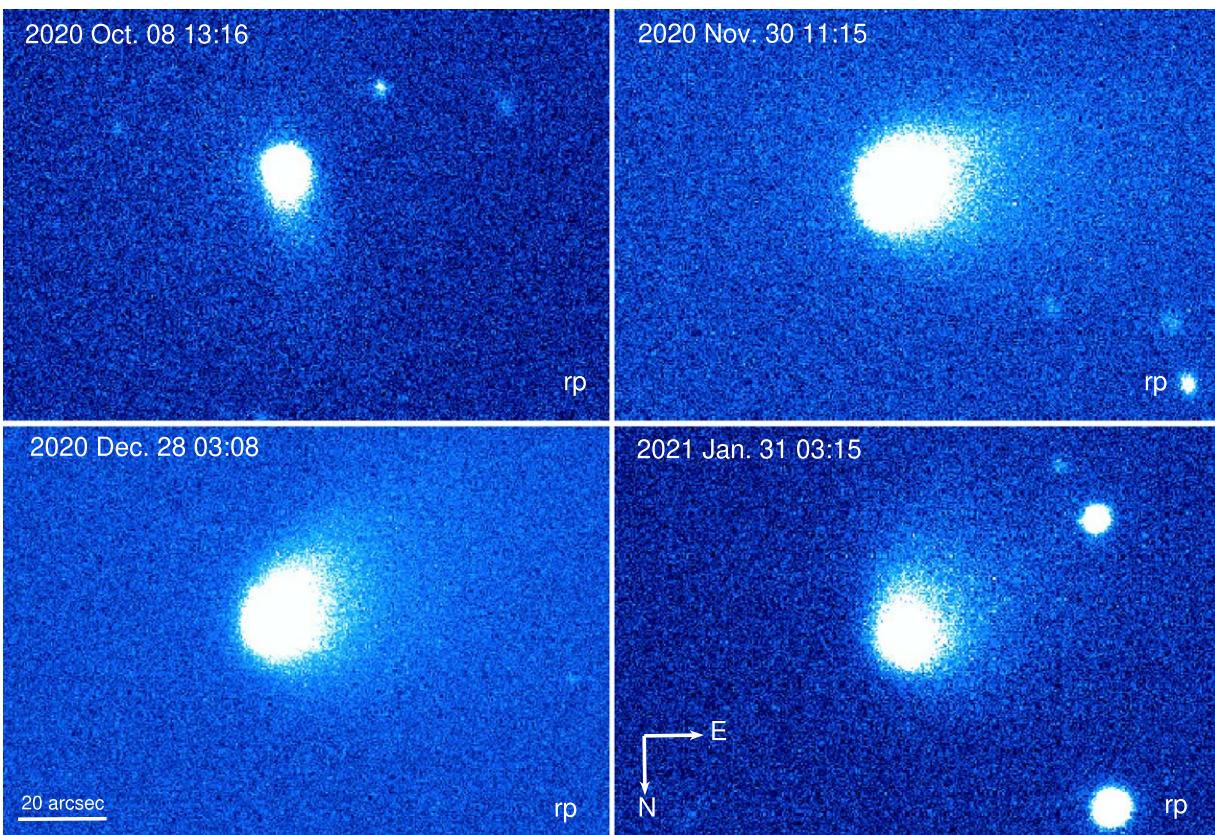


Figure 9. Evolution of 156P coma morphology before and after perihelion in r' images from LOOK. The orientation and scale are given at the bottom of the lower panels.

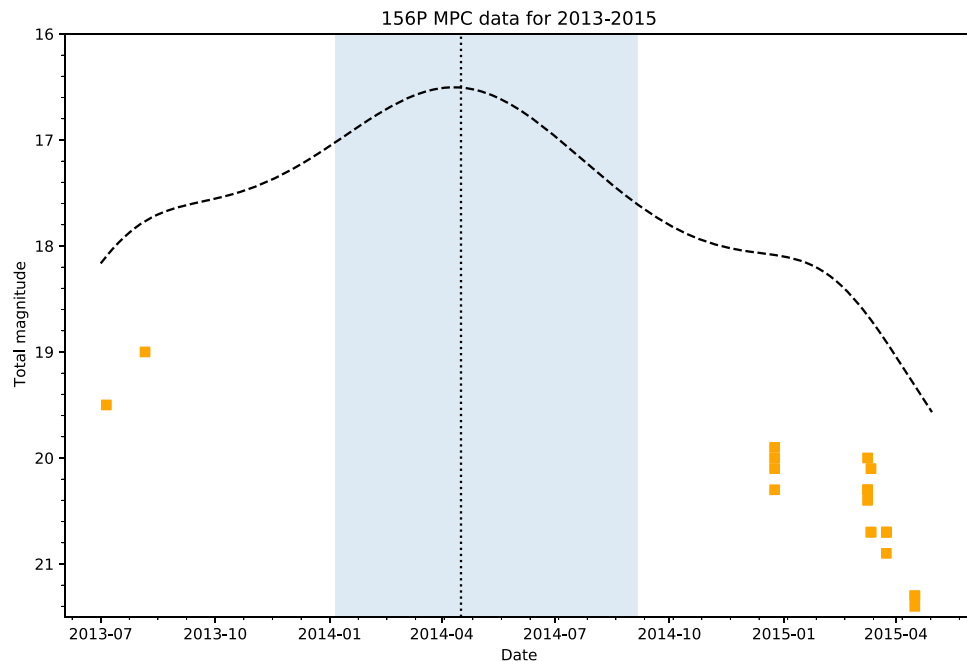


Figure 10. Total magnitudes for 156P from the Minor Planet Center database (orange squares) for the 2013–2015 apparition, along with the predicted total magnitude from JPL Horizons (black dashed line). The time of perihelion is indicated by the vertical dotted line, and the time when the solar elongation was $<40^\circ$ is shown by the blue shaded area.

significantly (~ 1.25 mag) fainter than expected based on the JPL fit to the 1993–2022 data alone (which is dominated by the large number of post-2020 observations). This may have contributed to the dearth of observations reported over the

approximately 16 months around perihelion, along with a long period of unobservability when the comet was close to the Sun. We speculate that the increased activity of 156P in 2020 may have been initiated by the orbit change since the previous

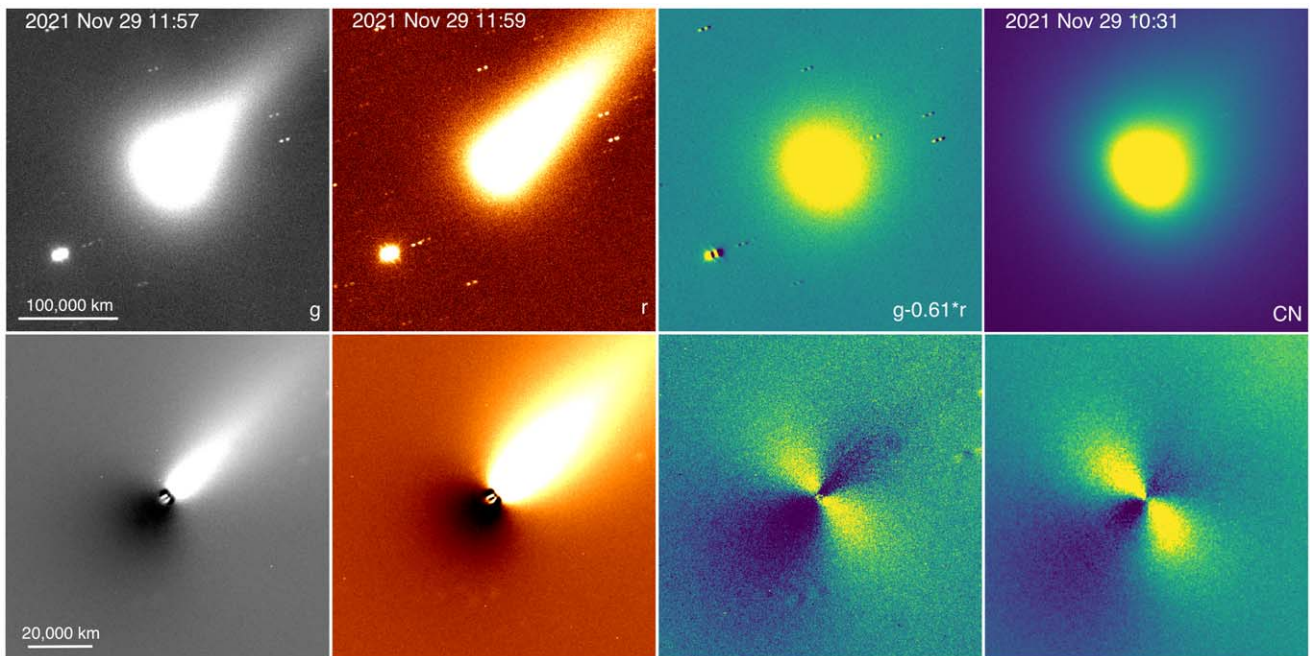


Figure 11. Unenhanced (top row) and enhanced (bottom row) images of C/2021 A1 (Leonard) in various filters on 2021 November 29. All images are centered on the opto-center of the comet and have north up and east to the left. All images in the top row are 325,000 km across, while all images in the bottom row are 100,000 km across and have been enhanced by subtraction of an azimuthal median profile. Light is bright and dark is faint in all panels. The first and second panels in each row are the g' and r' images, respectively, and the third panel in each row is a synthetic “gas” image created by scaling an r' image (median of all images taken that night) by the estimated dust color and subtracting this scaled image from a median g' image. As discussed in the text, the morphology of this synthetic gas image closely matches that of the CN gas image (fourth column; acquired by B. Skiff using the Lowell Observatory 42-inch telescope) and is very different from the “dust” (r' -band) image. Two jets can be seen oriented near positional angles 40° and 220° in the enhanced gas images, while the tail is to the northwest in the dust images. A very faint residual dust tail is still seen near the northwest corner in the gas images.

perihelion passage in 2014 April. Some possible mechanisms for the increased activity include increased insolation and resulting deeper propagation of the thermal wave or a shift in the pole orientation that has resulted in changing seasonal illumination of the source regions. Another possibility is that a torque was applied to the nucleus owing to the close approach to Jupiter that rearranged/exposed previously buried volatiles, although this seems somewhat unlikely given the nominal close approach distance of 0.36 au.

C/2021 A1 (Leonard). Oort Cloud comet C/2021 A1 (Leonard) reached perihelion on 2022 January 3 at $q = 0.615$ au. Although Leonard is not a DNC, we included it in our sample since its heliocentric distance changed by nearly a factor of 6 between our earliest observation on 2021 May 25 and perihelion, making it a good target for comparison with DNC brightness evolution. Its generally small solar elongation near perihelion prevented extensive observations from any one facility, but a brief window before perigee (0.23 au on 2021 December 12) allowed regular monitoring with LCO, and we obtained 13 epochs of g' and r' imaging from 2021 November 6 to December 6.

C/2021 A1 displayed distinctly different morphology between g' and r' when it was brightest in late 2021, prior to perihelion on 2022 January 03. Since the g' filter contains bright C_2 emission bands and fainter C_3 emission bands (see Figure 3), while r' is free of bright emission bands, we constructed a synthetic “gas” image by scaling an r' image and subtracting it from the contemporaneously obtained g' image. The scaling was conducted by eye, with the scaling coefficient determined by looking for the disappearance of the dust tail in the “gas” image. The best determined value was 0.61, but values within ± 0.02 produced indistinguishable results. The scale images were in flux units

calibrated via the AB magnitude system (i.e., $F_v(g') - 0.61 \times F_v(r')$); converting from flux to magnitudes implies that the dust color was $g_{P1} - r_{P1} = 0.54 \pm 0.05$ mag, including calibration uncertainties. Smaller scaling coefficients resulted in a visible excess of positive (g') tail, while larger scaling coefficients resulted in an excess of negative (r') tail; our final scaling coefficient choice varied from night to night, but the resulting morphology was essentially unchanged for values within 0.02 mag. In Figure 11, we show example g' and r' images from 2021 November 29 ($r_h = 0.95$ au, $\Delta = 0.58$ au). The LCO telescope used was not optimally focused at the time of the data acquisition, but the broad structures (coma and tail) are not adversely affected. The dust color, $g_{P1} - r_{P1} = 0.54$ mag, is considerably redder than the total coma color measured within a 5000 km ($10''$) radius aperture: $g_{P1} - r_{P1} = 0.21 \pm 0.04$ mag. This implies that the gas contamination is $\sim 26\%$ in the g' filter for this observation and aperture size. TRAPPIST narrowband observations on 2021 December 19 show that the comet has dust-to-gas ratio typical of most comets, with an OH-to-dust $Af\rho$ production rate ratio of $Q(\text{OH})/Af\rho = 9 \times 10^{25}$ molecules $\text{s}^{-1} \text{cm}^{-1}$ (Jehin et al. 2021).

Figure 11 also shows an image taken 1.5 hr earlier using the narrowband CN filter from the HB comet filter set (Farnham et al. 2000) with Lowell Observatory’s 42-inch telescope and provided by B. Skiff. The gas morphology can be compared with that seen in our best synthetic “gas” image by looking at the last two panels of the bottom row. Both images are 100,000 km across, centered on the opto-center, and have been enhanced by subtraction of an azimuthal median in order to remove the bulk brightness and emphasize subtle brightness variations. This reveals two apparent gas jets of comparable

brightness and extent, one to the northeast and the other to the southwest. Although the CN image shown has not been properly decontaminated of dust, previous work (Knight & Schleicher 2011) has found that the dust contamination is negligible for comets with “typical” gas-to-dust ratios like Leonard. Furthermore, CN and C₂ coma morphologies tend to be very similar (e.g., Knight & Schleicher 2013; Knight et al. 2021), so a first-order comparison is reasonable to assess the technique. The figure also shows our g' and r' images at the same scale and enhanced by the same technique. The dust morphology is completely different from the gas, being dominated by the tail toward the northwest.

The orientation and extent of the jets are similar in both images, giving us confidence that the technique is useful for a qualitative assessment of gas in sufficiently bright comets. Small variations within a few thousand kilometers of the center are artifacts of the processing and image quality and should be ignored. There are subtle variations in the jet morphology, with the CN jets tilting slightly toward the southeast (in the sunward direction), while our “gas” jets show a slight tilt toward the northwest (in the tailward direction). It is possible that these differences are real and indicative of rotational variations during the intervening 1.5 hr, but they might also be due to the different gas species involved or to the processing technique. The ability of this technique to monitor rotational variation of gas morphology will be explored in a future paper; for now we simply note that it appears viable.

7. Discussion and Conclusions

We have described the scientific goals and motivation for the LCO Outbursting Objects Key (LOOK) Project, a 3 yr, long-term status proposal on the LCO network, along with details on our target selection, monitoring, outburst response, and data reduction steps. We have also outlined some of the initial results from the first ~ 16 months of operation.

Completion of observing (at the end of 2023 July) and comprehensive analysis of the full 3 yr data set will be needed before we can make definitive statements on the behavior of DNCs, specifically with regard to changes in activity with distance from the Sun. These results will be valuable to feed into the planning and target selection for ESA’s Comet Interceptor mission to visit, ideally, a DNC after launch in 2029. A more complete understanding of the evolution of the activity behavior of DNCs as a function of distance and target properties could aid the determination of the best target for Comet Interceptor should we find ourselves in the fortunate situation of having a choice of targets that are reachable by the spacecraft. Raw and BCD images and data products from the LOOK observing program, as with all data taken on the LCO network, are available from the public LCO Science Archive as detailed in the acknowledgments. Additional data such as spectra from other facilities and catalogs of derived properties such as photometry will be made available from the LOOK project website following publication of papers containing the data or the end of the observing program.

The recent discovery of two confirmed interstellar objects (1I/‘Oumuamua and 2I/Borisov) and the very large diameter C/2014 UN₂₇₁ (Bernardinelli–Bernstein), along with its activity even at large heliocentric distances, shows the potential of what can be discovered through the combination of large-area sky surveys coupled with rapid data reduction, analysis, and alert generation. This potential is driving a lot of the

development of survey and analysis strategy for the Vera C. Rubin Observatory and how its Legacy Survey of Space and Time (LSST) will be carried out. In addition, it is driving thinking and evolution of the transient follow-up ecosystem for existing and future surveys such as LSST, including developments such as the Astrophysical Events Observatories Network (AEON; Street et al. 2020). The first iteration of AEON, with the use of the SOAR 4.1 m telescope in Chile being scheduled in a remote queue mode along with the rest of the LCO network by the LCO scheduler, has already been successfully utilized by LOOK project members to study fainter DNCs (preliminary results were presented by Holt et al. 2021). As shown in Section 4.1, there is also great potential for integrating classically scheduled and operated telescopes into a follow-up ecosystem to provide additional observational resources for follow-up. Coordinated observations and management of large observing programs utilizing robotic (LCO), partially queue-based (SOAR), and nonrobotic telescopes (Mount John) is possible through a TOM system as discussed in Section 4.

The LOOK Project data set so far, presented here, demonstrates that small transient events may be readily discovered and studied in cometary comae with the LCO network. As discussed in Section 6.3.2, 28 outbursts of 14 comets have been discovered or studied in the first ~ 16 months of the LOOK Project. In addition to these outbursts of the more heavily monitored and larger sample of bright comets, we have also presented evidence of quiescent activity on an active asteroid (Section 6.3.1) and outbursts on a Centaur (Section 6.3.3). These outburst detections are primarily coming from ZTF, which covers the northern sky in two bands every two nights, supplemented by outburst discoveries from LOOK data and personnel analysis, as well as amateur observers. Although there is a generalized alert system for ZTF (Patterson et al. 2019) that should include active asteroids and comets, in the desire to avoid sending alerts for image artifacts and the bias toward stellar science within ZTF, this means that extended objects such as comets or activated asteroids are filtered out of the alert stream. This reinforces the need for the next generation of alert brokers (e.g., Narayan et al. 2018; Smith et al. 2019; Förster et al. 2021) for Rubin Observatory to be able to handle all science cases, including moving and extended objects. There is the strong possibility of additional alerts for the southern sky to come from the ATLAS 3 and 4 telescopes in Chile and South Africa with their entrance into regular operations during 2022. Although there is not a general alert system for ATLAS, we can expect an increased number of outburst discoveries in the Southern Hemisphere, where LCO has more telescopes and a more even longitudinal spread of telescopes, allowing a more rapid response and continuous coverage of outbursts.

Although COVID-19 pandemic-related delays have pushed the start of survey operations and alert generation from the Rubin Observatory beyond the end date of the LOOK Project, the discovery of new exceptional objects (such as C/2014 UN₂₇₁ Bernardinelli–Bernstein) and the alerts from the already-operating surveys (or those that will start soon) will provide valuable targets and input for developing, operating, and testing the broader transient follow-up infrastructure for planetary science in preparation for the era of a larger volume of objects and alerts once Rubin observations start. The determination of the rate, behavior, and evolution of outbursts on the variety of solar system objects covered by LOOK, along with

characterization of the onset and evolution of activity on DNCs, will form a valuable resource for the future.

We appreciate the work and dedication of the amateur astronomical community and their contributions to the study of transient phenomena in small solar system objects. We thank Brian Skiff for providing the CN image of C/2021 A1 Leonard.

M.S.P.K. and S.P. acknowledge support from the NASA Solar System Observations program (80NSSC20K0673). M.T. B. appreciates support by the Rutherford Discovery Fellowships from New Zealand Government funding, administered by the Royal Society Te Apārangi. M.E.S., M.M.D., and C.S. were supported in part by the UK Science Technology Facilities Council (STFC) grants ST/V000691/1, ST/V506990/1, and ST/V000586/1, respectively. M.M.K. was supported by NASA Solar System Observations program grant 80HQTR20T0060. Development of NEOexchange was funded in part by the NASA Near Earth Objects Observations program through grants NNX14AM98G and 80NSSC18K0848 to Las Cumbres Observatory (LCO).

This work makes use of observations from the Las Cumbres Observatory global telescope network. Observations with the LCOGT 1 m were obtained as part of the LCO Outbursting Objects Key (LOOK) Project (KEY2020B-009). Some observations in this paper are based on observations made with the MuSCAT3 instrument, developed by the Astrobiology Center and under financial supports by JSPS KAKENHI (JP18H05439) and JST PRESTO (JPMJPR1775), at Faulkes Telescope North on Maui, HI, operated by the Las Cumbres Observatory. TRAPPIST-South is a project funded by the Belgian Fonds (National) de la Recherche Scientifique (F.R.S.-FNRS) under grant PDR T.0120.21. TRAPPIST-North is a project funded by the University of Liège, in collaboration with the Cadi Ayyad University of Marrakech (Morocco). E. Jehin is FNRS Senior Research Associate.

This research has made use of data and services provided by the International Astronomical Union's Minor Planet Center.

This research has made use of NASA's Astrophysics Data System Bibliographic Services. Data Access: Raw Data Products (and Basic Calibrated Data products as described in Section 5) supporting this study are available from the LCO Science Archive at <https://archive.lco.global> using the KEY2020B-009 proposal code following a 12-month embargo/proprietary period.

Facilities: LCOGT, FTN, MtJohn:1.8 m, TRAPPIST.

Software: astropy (Astropy Collaboration et al. 2018), sbpy (Mommert 2019), astroquery (Ginsburg et al. 2019), JPL Horizons (Giorgini et al. 1996), SEP (Barbary 2016), DS9 (Joye & Mandel 2003), reproject (Robitaille 2018), photutils (Bradley et al. 2021), calviacat (Kelley & Lister 2021), ccdproc (Craig et al. 2021), BANZAI (McCully et al. 2018).

ORCID iDs

Tim Lister <https://orcid.org/0000-0002-3818-7769>
 Michael S. P. Kelley <https://orcid.org/0000-0002-6702-7676>
 Carrie E. Holt <https://orcid.org/0000-0002-4043-6445>
 Henry H. Hsieh <https://orcid.org/0000-0001-7225-9271>
 Michele T. Bannister <https://orcid.org/0000-0003-3257-4490>
 Aayushi A. Verma <https://orcid.org/0000-0003-2396-4569>
 Matthew M. Dobson <https://orcid.org/0000-0002-1105-7980>
 Matthew M. Knight <https://orcid.org/0000-0003-2781-6897>

Youssef Moulane <https://orcid.org/0000-0001-9784-6886>
 Megan E. Schwamb <https://orcid.org/0000-0003-4365-1455>
 Dennis Bodewits <https://orcid.org/0000-0002-2668-7248>
 James Bauer <https://orcid.org/0000-0001-9542-0953>
 Joseph Chatelain <https://orcid.org/0000-0002-1278-5998>
 Estela Fernández-Valenzuela <https://orcid.org/0000-0003-2132-7769>
 Daniel Gardener <https://orcid.org/0000-0002-9925-0426>
 Emmanuel Jehin <https://orcid.org/0000-0001-8923-488X>
 Rosita Kokotanekova <https://orcid.org/0000-0003-4617-8878>
 Eva Lilly <https://orcid.org/0000-0002-7696-0302>
 Man-To Hui <https://orcid.org/0000-0001-9067-7477>
 Adam McKay <https://orcid.org/0000-0002-0622-2400>
 Cyrielle Opitom <https://orcid.org/0000-0002-9298-7484>
 Silvia Protopapa <https://orcid.org/0000-0001-8541-8550>
 Ryan Ridden-Harper <https://orcid.org/0000-0003-1724-2885>
 Charles Schambeau <https://orcid.org/0000-0003-1800-8521>
 Colin Snodgrass <https://orcid.org/0000-0001-9328-2905>
 Helen Usher <https://orcid.org/0000-0002-8658-5534>
 Kacper Wierzbos <https://orcid.org/0000-0002-4884-9367>
 Quanzhi Ye (叶泉志) <https://orcid.org/0000-0002-4838-7676>
 Edward Gomez <https://orcid.org/0000-0001-5749-1507>
 Sarah Greenstreet <https://orcid.org/0000-0002-4439-1539>

References

- A'Hearn, M. F., Belton, M. J. S., Delamere, W. A., et al. 2011, *Sci*, **332**, 1396
 A'Hearn, M. F., Millis, R. C., Schleicher, D. O., Osip, D. J., & Birch, P. V. 1995, *Icar*, **118**, 223
 A'Hearn, M. F., Schleicher, D. G., Millis, R. L., Feldman, P. D., & Thompson, D. T. 1984, *AJ*, **89**, 579
 Astropy Collaboration, Price-Whelan, A. M., Sipőcz, B. M., et al. 2018, *AJ*, **156**, 123
 Barbary, K. 2016, *JOSS*, **1**, 58
 Bellm, E. C., Kulkarni, S. R., Graham, M. J., et al. 2019, *PASP*, **131**, 018002
 Bernardinelli, P., & Bernstein, G. 2021, *MPEC*, **2021**, M53
 Bernardinelli, P. H., Bernstein, G. M., Montet, B. T., et al. 2021, *ApJL*, **921**, L37
 Bodewits, D., Kelley, M. S., Li, J. Y., et al. 2011, *ApJL*, **733**, L3
 Bradley, L., Sipőcz, B., Robitaille, T., et al. 2021, *astropy/photutils*: v1.1.0, Zenodo, doi:10.5281/zenodo.4624996
 Brown, T. M., Baliber, N., Bianco, F. B., et al. 2013, *PASP*, **125**, 1031
 Buzzi, L., Demetz, L., Aletti, A., et al. 2021, *CBET*, 4989, 1
 Chambers, K. C., Magnier, E. A., Metcalfe, N., et al. 2016, arXiv:1612.05560
 Chandler, C. O., Trujillo, C. A., & Hsieh, H. H. 2021, *ApJL*, **922**, L8
 Cochran, A. L., & Cochran, W. D. 2002, *Icar*, **157**, 297
 Craig, M., Crawford, S., Seifert, M., et al. 2021, *astropy/ccdproc*: v2.2.0—Image combination performance, v2.2.0, Zenodo, doi:10.5281/zenodo.4883632
 Di Sisto, R. P., & Rossignoli, N. L. 2020, *CeMDA*, **132**, 36
 Dobson, M., Fitzsimmons, A., Schwamb, M. E., et al. 2021a, *ATel*, **14903**, 1
 Dobson, M. M., Schwamb, M. E., Fitzsimmons, A., et al. 2021b, *RNAAS*, **5**, 211
 Duncan, M. J., & Levison, H. F. 1997, *Sci*, **276**, 1670
 Dybczyński, P. A., & Breiter, S. 2022, *A&A*, **657**, A65
 Dybczyński, P. A., & Królikowska, M. 2015, *MNRAS*, **448**, 588
 Eastman, J. D., Brown, T. M., Hygelund, J., et al. 2014, *Proc. SPIE*, **9147**, 914716
 Farnham, T. 2021, *ATel*, **14759**, 1
 Farnham, T. L., Schleicher, D. G., & A'Hearn, M. F. 2000, *Icar*, **147**, 180
 Farnham, T. L., Wellnitz, D. D., Hampton, D. L., et al. 2007, *Icar*, **187**, 26
 Feaga, L. M., A'Hearn, M. F., Sunshine, J. M., Groussin, O., & Farnham, T. L. 2007, *Icar*, **190**, 345
 Fitzsimmons, A., Erasmus, N., Thirouin, A., Hsieh, H. H., & Green, D. W. E. 2021, *CBET*, 4995, 1
 Fitzsimmons, A., Weryk, R., Yoshimoto, K., et al. 2020, *CBET*, 4895, 1
 Förster, F., Cabrera-Vives, G., Castillo-Navarrete, E., et al. 2021, *AJ*, **161**, 242

- Gaia Collaboration, Brown, A. G. A., Vallenari, A., et al. 2021, *A&A*, **649**, A1
- Ginsburg, A., Sipőcz, B. M., Brasseur, C. E., et al. 2019, *AJ*, **157**, 98
- Giorgini, J. D., Yeomans, D. K., Chamberlin, A. B., et al. 1996, AAS/DPS Meeting, 28, 25.04
- Guilbert-Lepoutre, A. 2012, *AJ*, **144**, 97
- Henden, A. A., Templeton, M., Terrell, D., et al. 2016, *yCat*, **2336**, 0
- Holt, C. E., Knight, M. M., Lister, T., et al. 2021, AAS/DPS Meeting, **53**, 210.14
- Hsieh, H. H., Chandler, C. O., Denneau, L., et al. 2021, *ApJL*, **922**, L9
- Hsieh, H. H., Jewitt, D. C., & Fernández, Y. R. 2004, *AJ*, **127**, 2997
- Hsieh, H. H., Meech, K. J., & Pittichová, J. 2011, *ApJL*, **736**, L18
- Huebner, W. F., Benkhoff, J., Capria, M. T., et al. 2006, Heat and Gas Diffusion in Comet Nuclei (Noordwijk: ESA)
- Hughes, D. W. 1990, *QJRAS*, **31**, 69
- Ishiguro, M., Kuroda, D., Hanayama, H., et al. 2016, *AJ*, **152**, 169
- Ivezic, Ž., Kahn, S. M., Tyson, J. A., et al. 2019, *ApJ*, **873**, 111
- Jacobson, S. A., Marzari, F., Rossi, A., Scheeres, D. J., & Davis, D. R. 2014, *MNRAS*, **439**, L95
- Jehin, E., Gillon, M., Queloz, D., et al. 2011, *Msngr*, **145**, 2
- Jehin, E., Moulane, Y., & Manfroid, J. 2021, *ATel*, **15128**, 1
- Jehin, E., Moulane, Y., Manfroid, J., Pozuelos, F., & Hutsemekers, D. 2020, *ATel*, **14101**, 1
- Jewitt, D. 2009, *AJ*, **137**, 4296
- Jewitt, D., Agarwal, J., Li, J., et al. 2014, *ApJL*, **784**, L8
- Jewitt, D., Hsieh, H., & Agarwal, J. 2015, in Asteroids IV, ed. P. Michel, F. E. DeMeo, & W. F. Bottke (Tucson, AZ: Univ. Arizona Press), 221
- Jewitt, D., Weaver, H., Mutchler, M., Larson, S., & Agarwal, J. 2011, *ApJL*, **733**, L4
- Jewitt, D. C. 2004, in Comets II, ed. M. C. Festou, H. U. Keller, & H. A. Weaver (Tucson, AZ: Univ. Arizona Press), 659
- Joye, W. A., & Mandel, E. 2003, in ASP Conf. Ser. 295, Astronomical Data Analysis Software and Systems XII, ed. H. E. Payne, R. I. Jedrzejewski, & R. N. Hook (San Francisco, CA: ASP), 489
- Kelley, M., & Lister, T. 2021, *mkcelley/calviacat*: v1.2.0, Zenodo, doi:10.5281/zenodo.5061298
- Kelley, M. S. P. 2021, *ATel*, **14876**, 1
- Kelley, M. S. P., Bodewits, D., Ye, Q., et al. 2019, in ASP Conf. Ser. 523, Astronomical Data Analysis Software and Systems XXVII, ed. P. J. Teuben, M. W. Pound, B. A. Thomas, & E. M. Warner (San Francisco, CA: ASP), 471
- Kelley, M. S. P., Farnham, T. L., Li, J.-Y., et al. 2021a, *PSJ*, **2**, 131
- Kelley, S. P., Kokotanekova, R., Holt, C. E., et al. 2022, *ApJL*, in press
- Kelley, M. S. P., Lin, Z.-Y., Sharma, K., et al. 2021b, *CBET*, 4997, 2
- Kelley, M. S. P., & Lister, T. 2021, *ATel*, **14486**, 1
- Kelley, M. S. P., Lister, T., & Holt, C. E. 2021c, *ATel*, **14917**, 1
- Kelley, M. S. P., Lister, T., Sharma, K., et al. 2021d, *ATel*, **14565**, 1
- Kelley, M. S. P., Lister, T., Sharma, K., et al. 2021e, *ATel*, **14618**, 1
- Kelley, M. S. P., Lister, T., Sharma, K., et al. 2021f, *CBET*, 4996, 1
- Kelley, M. S. P., Lister, T., Sharma, K., et al. 2021g, *ATel*, **15016**, 1
- Kelley, M. S. P., Lister, T., Sharma, K., et al. 2021h, *ATel*, **15052**, 1
- Kelley, M. S. P., Lister, T., Sharma, K., et al. 2021i, *ATel*, **14940**, 1
- Kelley, M. S. P., Sharma, K., Bhalerao, V., Anupama, G. C., & Barway, S. 2021j, *ATel*, **14628**, 1
- Kelley, M. S. P., Sharma, K., Kumar, H., et al. 2021k, *ATel*, **14787**, 1
- Kelley, M. S. P., Sharma, K., Swain, V., et al. 2021l, *ATel*, **15053**, 1
- Knight, M. M., & Schleicher, D. G. 2011, *AJ*, **141**, 183
- Knight, M. M., & Schleicher, D. G. 2013, *Icar*, **222**, 691
- Knight, M. M., Schleicher, D. G., & Farnham, T. L. 2021, *PSJ*, **2**, 104
- Kokotanekova, R., Lister, T., Bannister, M., et al. 2021, *ATel*, **14733**, 1
- Kronk, G. W. 2003, Cometography: A Catalog of Comets, 2 (Cambridge: Cambridge Univ. Press), 1800
- Lauretta, D. S., Hergenrother, C. W., Chesley, S. R., et al. 2019, *Sci*, **366**, 3544
- Le Roy, L., Altwegg, K., Balsiger, H., et al. 2015, *A&A*, **583**, A1
- Lellouch, E., Moreno, R., Bockelée-Morvan, D., Biver, N., & Santos-Sanz, P. 2022, *A&A*, **659**, L1
- Levison, H. F., Bottke, W. F., Gounelle, M., et al. 2009, *Natur*, **460**, 364
- Li, J., Jewitt, D., Clover, J. M., & Jackson, B. V. 2011, *ApJ*, **728**, 31
- Lister, T. A., Gomez, E., Chatelain, J., et al. 2021, *Icar*, **364**, 114387
- McCully, C., Volgenau, N. H., Harbeck, D. R., et al. 2018, *Proc. SPIE*, **10707**, 107070K
- McNaught, R. 2003, *IAUC*, **8118**, 1
- Meech, K. J., Kleyana, J. T., Hainaut, O., et al. 2017, *ApJL*, **849**, L8
- Meech, K. J., Pittichová, J., Bar-Nun, A., et al. 2009, *Icar*, **201**, 719
- Mommert, M., Kelley, P., de Val-Borro, M. S., et al. 2019, *JOSS*, **4**, 1426
- Morbidelli, A., & Nesvorný, D. 2020, in The Trans-Neptunian Solar System, ed. D. Prialnik, M. A. Barucci, & L. Young (Amsterdam: Elsevier), 25
- Moulane, Y., Jehin, E., Opitom, C., et al. 2018, *A&A*, **619**, A156
- Narayan, G., Zaidi, T., Soraisam, M. D., et al. 2018, *ApJS*, **236**, 9
- Narita, N., Fukui, A., Kusakabe, N., et al. 2019, *JATIS*, **5**, 015001
- Narita, N., Fukui, A., Kusakabe, N., et al. 2020, *Proc. SPIE*, **11447**, 114475K
- Opitom, C., Guilbert-Lepoutre, A., Jehin, E., et al. 2016, *A&A*, **589**, A8
- Patterson, M. T., Bellm, E. C., Rusholme, B., et al. 2019, *PASP*, **131**, 018001
- Prialnik, D., & Rosenberg, E. D. 2009, *MNRAS*, **399**, L79
- Ridden-Harper, R., Bannister, M. T., & Kokotanekova, R. 2021, *RNAAS*, **5**, 161
- Robitaille, T. 2018, reproject: Astronomical Image Reprojection in Python, v0.4, Zenodo, doi:10.5281/zenodo.1162674
- Rossi, A., Marzari, F., & Scheeres, D. J. 2009, *Icar*, **202**, 95
- Sako, T., Sekiguchi, T., Sasaki, M., et al. 2008, *ExA*, **22**, 51
- Schleicher, D. G., & Bair, A. N. 2011, *AJ*, **141**, 177
- Sharma, K., Kelley, M. S. P., Lister, T., et al. 2021a, *ATel*, **14984**, 1
- Sharma, K., Kelley, M. S. P., Stanzin, J., et al. 2021b, *ATel*, **14687**, 1
- Siverd, R. J., Brown, T. M., Barnes, S., et al. 2018, *Proc. SPIE*, **10702**, 107026C
- Smith, K. W., Williams, R. D., Young, D. R., et al. 2019, *RNAAS*, **3**, 26
- Snodgrass, C., Agarwal, J., Combi, M., et al. 2017, *A&ARv*, **25**, 5
- Snodgrass, C., & Jones, G. H. 2019, *NatCo*, **10**, 5418
- Stern, S. A. 2003, *Natur*, **424**, 639
- Street, R. A., Adamson, A., Blakeslee, J. P., et al. 2020, *Proc. SPIE*, **11449**, 1144925
- Tonry, J. L., Denneau, L., Flewelling, H., et al. 2018a, *ApJ*, **867**, 105
- Tonry, J. L., Denneau, L., Heinze, A. N., et al. 2018b, *PASP*, **130**, 064505
- Tonry, J. L., Stubbs, C. W., Lykke, K. R., et al. 2012, *ApJ*, **750**, 99
- Trigo-Rodríguez, J. M., García-Melendo, E., Davidsson, B. J. R., et al. 2008, *A&A*, **485**, 599
- Tseng, W. L., Bockelée-Morvan, D., Crovisier, J., Colom, P., & Ip, W. H. 2007, *A&A*, **467**, 729
- van Buitenen, G. 2021, *CBET*, 4997, 1
- Veverka, J., Klaasen, K., A'Hearn, M., et al. 2013, *Icar*, **222**, 424
- Vincent, J. B., A'Hearn, M. F., Lin, Z. Y., et al. 2016, *MNRAS*, **462**, S184
- Vincent, J. B., Hviid, S. F., Mottola, S., et al. 2017, *MNRAS*, **469**, S329
- Walsh, K. J., Morbidelli, A., Raymond, S. N., O'Brien, D. P., & Mandell, A. M. 2011, *Natur*, **475**, 206
- Whipple, F. L. 1978, *M&P*, **18**, 343
- Willmer, C. N. A. 2018, *ApJS*, **236**, 47
- Yang, B., Jewitt, D., Zhao, Y., et al. 2021, *ApJL*, **914**, L17
- Ye, Q., Kelley, M. S. P., Bodewits, D., et al. 2019, *ApJL*, **874**, L16